Recent progress in the CoCrNi alloy system

Sakshi Bajpai [a],[*], Benjamin E. MacDonald [a], Timothy J. Rupert [a], Horst Hahn [a],[b],
Enrique J. Lavernia [a], Diran Apelian [a]

[a] University of California, Irvine, CA 92697, USA
[b] Karlsruhe Institute of Technology, Karlsruhe 76021, Germany

A B S T R A C T

The exceptional mechanical properties, particularly at cryogenic temperatures, of the equiatomic CoCrNi alloy are documented in numerous published studies. Similar to the equiatomic CoCrFeMnNi (so called Cantor alloy), from which the ternary alloy was derived, the CoCrNi ternary possesses low stacking fault energy that promotes complex deformation modes, as well as the activation of deformation twinning at ambient temperatures and increased strain. In addition to outstanding deformation mechanisms, chemical short-range order and face-centered cubic (FCC)-hexagonal close packed (HCP) transitions have been verified in this alloy and prove to be key factors contributing to the alloy's notable properties. The relationship between stacking fault energy and FCC→HCP phase transitions has been developed over the years through other low stacking fault materials, but the question that arises is: do well established physical metallurgical mechanisms require modification when applied to systems such as CoCrNi given their compositional complexity? Local chemical order plays an important role in that it brings the deviation from the random solid solution behavior generally expected from complex concentrated alloys. In this review, the fundamental atomistic deformation mechanisms of the CoCrNi alloy will be reviewed with a focus on deformation substructures and chemical short-range ordering. Recent studies on microstructural engineering through thermo-mechanical processing and efforts to enhance the tensile properties of the CoCrNi derived systems with minor alloying additions are discussed. Finally, future directions of research, which involve applying current understanding of the underlying mechanisms towards alloy design strategies, are discussed.

1. Introduction

The development of high entropy alloys (HEAs) or so called complex concentrated alloys (CCAs) has become a predominate class within the field of materials science. The field's understanding of HEAs evolved significantly over the last two decades and has led to the development of alloys which might be future replacements for the existing conventional materials, such as high-strength steels and nickel-based superalloys [1,2]. One of these CCAs is the equiatomic CoCrNi, known for its excellent combination of tensile strength, ductility, and fracture resistance especially at cryogenic temperature, which will be discussed in detail in this review. This section of the review is dedicated to the evolution of CCAs and how the ternary CoCrNi, a subset of the equiatomic CoCrFeMnNi Cantor alloy, emerged as a prominent CCA system.

Conventional alloying strategies, where elements are added in minor amounts to a base metal, have been the common approach of developing metallic alloys since the Bronze Age. In 2004, two individual research groups [3,4] introduced the concept of concentrated multicomponent alloys or HEAs which deviates from the solvent-solute paradigm. It was found that the equiatomic composition of multi-component alloys stabilized solid solution phases over intermetallic phases and led to simpler microstructures than originally expected. Yeh et al. [2] attributed this behavior to the high configurational mixing entropy of equiatomic multicomponent alloys. While the motivation behind HEAs was to explore the central region of the compositional space, most of the early research was focused on alloys with equiatomic composition that yielded relatively simple microstructures with minimal intermetallic content. To avoid the barriers posed by specific definitions, terms such as CCAs and multi principal element alloys (MPEAs) were coined thus removing the requirement that the number of components need to be greater than or equal to 5, or that the value of configurational entropy be greater than 1.5R [3]. This shift is seen in recent publications where a vast number of compositions with no limits on the minimum number of elements are being explored, both single-phase and multiphase in equiatomic, as well non-equiatomic ratios with an understanding that configurational entropy alone cannot determine the stability of phases and that the role of enthalpy must be considered [4–8]. In this review, the term CCAs will be used to address this class of multi-component alloys. Our understanding is that increasing the number of elements does
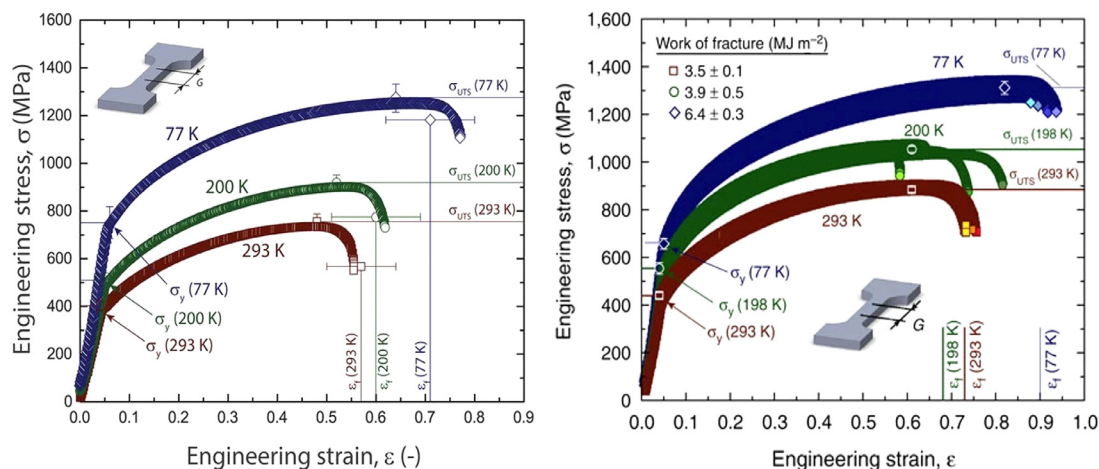
Fig. 1. Comparison of tensile properties of the equiatomic CoCrFeMnNi (left) and CoCrNi (right) from reference [11] and [15], respectively.

not necessarily result in improved properties. An example of this is the equiatomic CoCrFeMnNi Cantor alloy and its ternary derivates, particularly the equiatomic CoCrNi alloy. This alloy has become the focus of many investigations based on its unique mechanical properties which include tensile strength of ~1 GPa at failure strain of ~70%, and fracture-toughness above 200 MPa m$^{1/2}$. These properties synergistically increase even down to cryogenic temperatures which is attributed to a range of underlying mechanisms detailed in the next section.

CCAs with elemental 3d transition metals have been investigated by many researchers. Among them, the equiatomic CoCrFeMnNi was one of the earliest and most well-researched CCAs [9–11]. Since then, a significant amount of research has been conducted within this system exploring different alloying additions, non-equiatomic composition, mechanical behavior, corrosion behavior, and radiation damage tolerance [9]. The primary focus of studies on this alloy has been the mechanical properties, which show a room temperature yield strength of ~400 MPa and tensile strength of ~700 MPa and with an elongation of almost 56%. Gludovatz et al. highlighted the exceptional strength-ductility synergy in the equiatomic CoCrFeMnNi at cryogenic temperatures [11]. It was reported that as the temperature decreased from 293 K to 77 K, the yield strength and ultimate tensile strength increased by ~85% and ~70%, respectively with a simultaneous increase in the tensile ductility by ~25%. The fracture toughness of the quinary alloy was also found to have a crack initiation toughness of 200 MPa·m$^{1/2}$ or more which was retained even at cryogenic temperatures. These properties were attributed to the activation of deformation-induced nanotwins [12] as an additional deformation mechanism with the decreasing temperature giving rise to the dynamic Hall-Petch effect by introducing additional interfaces as well as delaying the onset of necking due to increased strain hardening.

In 2014, Wu et al. [13,14] investigated a total of ten binary, ternary, and quaternary subsets of the Cantor alloy with equiatomic compositions to understand their phase evolution and mechanical behavior. It was concluded that it is not just the number of elements but also the nature of elements that dictate the mechanical behavior of the CCAs, with Cr being a potent strengthener in the Cantor alloy family. Among all the subsets, this work highlighted the ternary CoCrNi alloy, with a single-phase FCC structure, having the highest strength and ductility in the temperature range of 77–673 K. This alloy was further studied by Gludovatz et al. [15] who observed activation of an additional deformation mode of nano twinning which led to a tensile strength of 1.3 GPa while displaying failure strains of 90% and fracture toughness of over 430 MPa m$^{1/2}$ at 77 K. Fig. 1 compares the tensile properties of the equiatomic CoCrFeMnNi and CoCrNi at different temperatures. The most prominent difference between the equiatomic CoCrFeMnNi and ternary CoCrNi is the activation of twinning at room temperature as an additional mode

of deformation in the latter. Activation of twinning increases as the temperature decreases or the strain increases.

Through the first section of this review, the current understanding of the atomistic mechanisms of the CoCrNi CCAs is discussed. Knowledge of stacking fault energy (SFE) and FCC→HCP phase transitions have been developed over the years through other low stacking fault materials however, the question that remains to be answered in the CoCrNi system is the role of compositional complexity. Accordingly, local chemical ordering and its effect on deformation mechanisms are discussed in detail. The next section of the review focuses on microstructural engineering to further enhance tensile properties of the CoCrNi alloy via thermo-mechanical processing. Lastly, derivative systems obtained by minor alloying additions to the base CoCrNi ternary are reviewed with an emphasis on their effect on mechanical properties.

2. Atomistic mechanisms driving mechanical behavior

The synergy between strength and ductility in the CoCrNi CCAs can be attributed to the underlying atomistic mechanisms. Besides that, the constituent elements also play an important in determining the mechanical properties. Since the individual elements In CoCrNi alloy have similar atomic radius, one would expect lattice distortion to be quite less. But counterintuitively, the solid solution strengthening effect in the ternary CoCrNi is found to be high [16]. It has been established that in case of CCAs, the lattice distortion and hence the solid solution strengthening effect is less related to the atomic radius and directly proportional to the atomic volume misfit and/or shear modulus [17]. The calculated atomic volumes for Co, Cr and Ni are respectively 11.12, 12.27 and 10.94 A^3 [17]. Hence, there is an appreciable volume misfit that leads to solid solution strengthening. Additionally, it has also been found that since Cr has a larger elastic modulus in FCC structures, Cr-containing alloys have higher shear modulus, which is the case with CoCrNi. That is why solid solution strengthening effect is high in CoCrNi. Another study by Oh et al. [18] highlights that a relatively large electronegativity difference between the individual atoms of Co, Cr and Ni also contribute to the increased solid solution strengthening effect in CoCrNi. All these effects together lead to the relatively high yield strength of the ternary CoCrNi alloy. While the effect of individual elements is significant, the mechanical behavior of these CCAs is heavily dependent on the atomistic mechanisms the are highlighted in detail in this section. We discuss the evolution of deformation substructures in the CoCrNi ternary alloy enabling it to overcome the strength-ductility tradeoff. The influence of SFE on the phase transition from FCC to HCP is then highlighted and the probability of a reverse HCP to FCC transition is reviewed. In the last part of this section, the presence of local chemical order within the CoCrNi alloy is discussed with an emphasis on how it can further affect
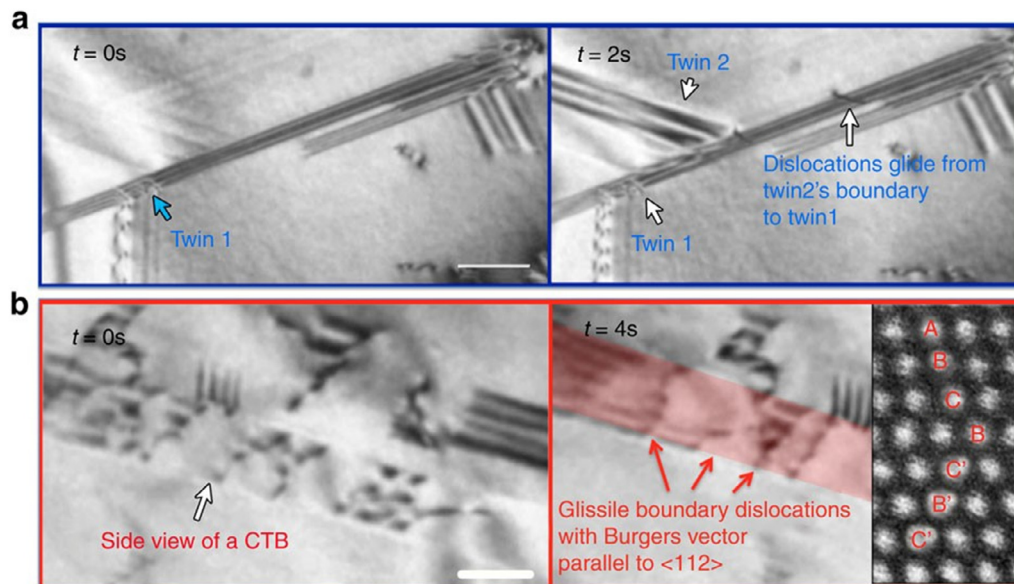
Fig. 2. (a) *In situ* transmission electron microscope (TEM) straining experiment showing the activation of multiple twins and their interaction with the dislocations, (b) TEM image of a stable twin boundary through which partial dislocations glide. The scale bar on both images: 200 nm [22].

SFE, deformation mechanisms, and eventually the mechanical properties.

2.1. Evolution of deformation substructures

The stacking fault energy (SFE) of a metal is a key factor in determining the dominant deformation mechanisms. In the case of face-centered cubic materials, when a perfect dislocation dissociates into two Shockley partials, the region between these two defects is a stacking fault (SF) and the energy associated with its formation is known as SFE. The width of a SF is inversely proportional to the SFE. The equiatomic CoCrNi alloy is a low SFE material with SFE between 18 and 45 mJ m^{-2}, similar to MP35N/ MP159 alloys, high-Mn austenitic twinning-induced plasticity (TWIP) steels and the CoCrFeMnNi Cantor alloys. The low SFE causes the SFs to be wide between the Shockley partials which makes cross slip energetically difficult and leads to activation of twinning as a secondary deformation mechanism. It is expected that as the SFE decreases, the deformation mechanisms change from dislocation glide to dislocation glide + twinning and further to dislocation glide + FCC→HCP phase transformation, or the ε-martensitic transformation in the case of steels [19,20], It is interesting that twinning in CCAs leads to a simultaneous increase in both tensile strength and ductility [21–24]. Twinning leads to the formation of a new interface that acts as an obstacle to dislocation motion, while also contributing to work hardening by delaying necking instability. Fig. 2(a) shows the activation of multiple twins in different directions and with different widths in CoCrNi during *in situ* straining experiments. Curtze and Kuokkala [20] suggested the formation of a 3D twin architecture inside individual grains (within the size range of ~5–50 microns) of an equiatomic CoCrNi alloy that stabilized the twin boundary even when the dislocations glide through it as shown in Fig. 2(b). Hence these twins contribute to plastic deformation while also strongly impeding dislocations therefore increasing the strength of the material.

The propensity for twinning increases with decreasing temperature and increasing strain. That is the reason why twinning activates as a secondary deformation mechanism in austenitic TWIP steels and in the Cantor alloys at lower temperatures (between 77 K to below RT) and at higher strain values [12,20]. On the other hand, the ternary CoCrNi shows twinning formation even at room temperature which further intensifies towards cryogenic temperatures. This behavior was attributed

to the SFE in equiatomic CoCrNi being 25% lower than that of the equiatomic CrMnFeCoNi and reflects in the mechanical properties of CoCrNi showing higher strength, ductility, and fracture toughness than the CrMnFeCoNi both at room temperature and cryogenic temperature [15,23]. There is a stark difference in experimental and predicted values of the SFE in the CoCrNi ternary alloy. While experimentally the SFE is estimated to be in the range of 18 ± 4 mJ m^{-2} [25] to 22 ± 4 mJ m^{-2} [23], the values calculated through first-principle calculations are generally negative: -24 mJ m^{-2} [22], or -41 mJ m^{-2} [26]. Simulations and calculations are generally performed at 0 K where the entropic contributions can be neglected, however at a finite temperature, e.g., room temperature, the atomic vibrations are appreciable enough to be considered while computing SFE values. This can be one explanation for the difference in experimental and simulated values. Also, it is worth mentioning that experimental measurements cannot be negative as the SFs observed during imaging have to be at finite distance to each other which will always lead to positive SFE values. Despite the inherent limitations of both experimental and theoretical approaches, such variation highlights that the compositional complexity of CCAs needs to be considered, as the variation in local atomic configuration will affect the SFs and corresponding SFE.

At the most fundamental level, SFE depends on the electron orbital interactions and the free electron density. For a pure FCC metal, it was demonstrated through ab-initio calculations [27] that for a metal like Cu, the charge distribution is nearly spherical which makes redistribution of electrons easy after shearing the close-packed plane to form a SF, hence reducing the energy penalty and leading to a low SFE value. On the other hand, Al has an angular charge distribution that poses difficulty in electron redistribution, giving rise to a high SFE value. Also, the d-electron density plays a significant role during shearing caused by the formation of SFs and hence plays an important role in determining SFE [28]. Moving from pure metal to conventional alloys, the addition of another element to the base element will also have its effect on the charge density distribution and atomic bonding. If an alloying element causes more charge accumulation, the directionality of metallic bonding is decreased which leads to a decrease in SFE and vice-versa. It was observed in the case of Co-based alloys [29] that the addition of Cr, W, and Mo leads to weaker atomic bonding due to increased charge distribution in the interstitial regions which in turn decreases the generalized SFE of Co. Whereas, Ni, Mn, Al, and Fe have the opposite effect and increase
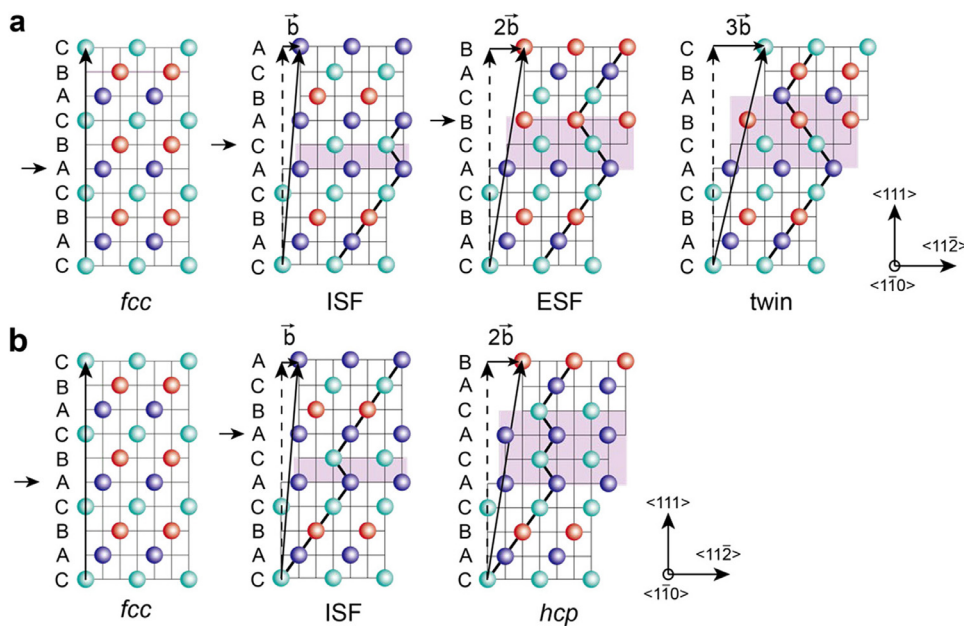
Fig. 3. Schematic showing the formation of twin and HCP phase from an (a) ESF and (b) ISF, respectively [32].

the generalized SFE of Co. Hence, every individual element has a unique effect on the SFE of the alloy and the same holds true for the CoCrNi alloy. Besides the electronic configurations, volume and magnetic effects also contribute to the determination of SFE and the same element may also have a different impact on a different base alloy [30]. This review, however, is concerned with the effect of alloying elements in the base CoCrNi ternary which is discussed in detail in a later section.

2.2. FCC→HCP phase transformation

Glide of a single Shockley partial on a closed pack plane in FCC stacking sequence generates an intrinsic stacking fault (ISF) whereas when the partial dislocations glide on two consecutive closed packed planes, an extrinsic stacking fault (ESF) is generated [31]. Fig. 3 shows how ESF leads to the formation of deformation twins while ISF serves as an embryo for the HCP phase [32]. Therefore, an ISF the FCC sequence can be seen as a layer of HCP stacking which can act as a favorable site for the growth of the HCP phase. The difference in energy of formation of these FCC and HCP phases can be related to the SFE. A low SFE suggests that the energy of formation of both FCC and HCP phases will be quite close to each other and other factors such as temperature and strain will stabilize one phase over another. Deformation-induced phase transformation, analogous to transformation-induced plasticity (TRIP) effect in steels [33], has been observed in other CCAs as well [34–37].

Compared to CoCrFeMnNi, where FCC→HCP phase transition was induced at high pressure [38], HCP phase formation seems to be more convenient in CoCrNi. Using spin polarized density functional theory (DFT) calculations [39], it was predicted that at 0 K, the HCP phase has lower energy than the FCC phase in CoCrNi. It can be reasoned that the higher Co (which is an HCP phase) content in CoCrNi alloy compared to CoCrFeMnNi stabilizes the HCP phase. A similar observation was made by Zhao et al. [40] in $CoCrNi_x$ alloys where single-phase FCC structure formed for x = 1 to 0.8 but as the Ni content decreased from x = 0.7 to 0.5, eventually increasing the Co content, both FCC and HCP phases coexisted. There is a higher probability of HCP phase formation in equiatomic ternary CoCrNi, than there is in the quinary CoCrFeMnNi. Niu et al. [26] rationalized this behavior by taking the magnetic frustration into account which is strong in the case of CoCrFeMnNi resulting in comparable FCC and HCP energies and hence no driving force for HCP transformation. In the case of CoCrNi, however, even if one considers

magnetic effects the HCP phase remains more stable than the FCC at lower temperatures.

For the equiatomic CoCrNi alloy, Miao et al. [39] reported a similar FCC to HCP phase transformation at higher strain levels both at room and cryogenic temperatures. The deformation substructure followed an expected pattern where at lower strain mainly planar dislocation slip existed and with increasing strain, nanotwins and HCP phase evolved and dominated the deformation. This work highlighted the formation of nanotwin-HCP lamella as shown in Fig. 4, suggesting that the HCP phase forms due to the interaction of the SFs and nanotwins. The HCP phase grows and remains localized in this interaction zone throughout. Even though the volume fraction of the HCP phase increases with increasing strain, more so at the cryogenic temperature than at RT, it should be noted that the highest amount of HCP phase detected by this work is only ~3% in a sample deformed to 53% true strain at cryogenic temperature. Another large-scale molecular dynamics simulation study by Yuan et al. [41] showed the HCP phase formed due to nucleation and propagation of multiple SFs at adjacent slip planes from the same grain boundary. The HCP phase in CoCrNi CCAs can be an additional strengthening mechanism in CoCrNi based alloys and can have a synergistic effect in improving the mechanical properties [42].

Contrary to TRIP steels, where a large fraction of FCC austenite transforms to HCP ε-martensite [43], the volume of transformed HCP phase in CoCrNi ternary alloy is quite low. This happens despite the sufficient driving force due to combined combination of low SFE, temperature and high strain. In their work, Niu et al. [26] suggest that the mixed dislocations trapped at the interface of the HCP region may facilitate the formation of new Shockley partials, causing the structure to heal back to its original FCC form. This explanation needs to be validated by further study. Previously, such reverse phase transformation from HCP to FCC has been suggested in another CCA system [36] $Fe_{50}Mn_{30}Co_{10}Cr_{10}$, where the bidirectional phase transformation was attributed to local dissipative heating and stress-strain fields acting as the driving force for HCP to FCC transformation.

While there are no reports of any HCP to FCC transformation in bulk CoCrNi, magnetron sputtered thin films of CoCrNi undergo a reverse transformation from HCP to FCC [44,45] when subjected to *in situ* tensile testing. Chen et al. [44] attribute this bidirectional FCC→HCP→FCC transformation to the small SFE of CoCrNi alloy and hence the flexible stacking sequence which gives the unique capability of facile slip on the close-packed $\{111\}_{FCC} \parallel (0\,0\,01)_{HCP}$ planes in both FCC and HCP
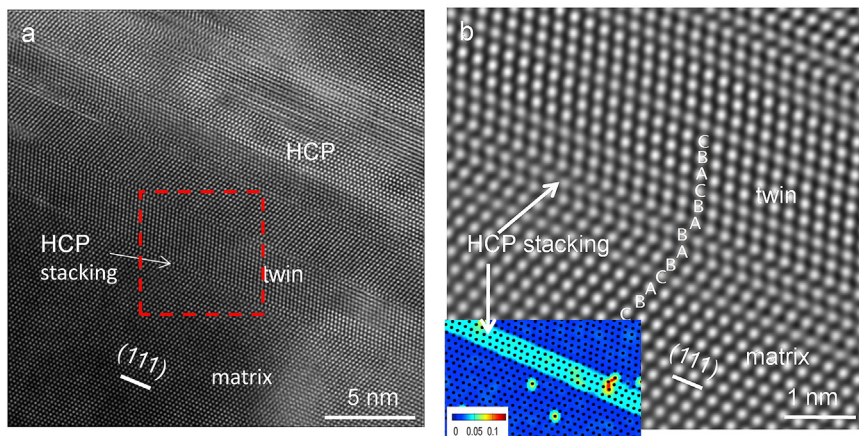
Fig. 4. Annular dark field (ADF) – scanning transmission electron microscope (STEM) image of CoCrNi specimen tested to 53% true strain at cryogenic temperature showing HCP band forming near the twin boundary. The inset in (b) is the center of symmetry (COS) map also highlighting HCP stacking [39].

phases of the CoCrNi alloy. It is to be noted that the reversible phase transformation occurs mostly near the central region of the micropillars which undergoes the highest deformation through shear banding during *in situ* testing. In another similar work Chen et al. [45] showed the dependency of deformation on the size of the pillars where high shear stress in sub-micron pillar can be enough to facilitate a lattice rotation along the basal plane of the HCP phase causing an increase in resolved shear stress and the glide of partial on every other basal plane of HCP stacking promoting the phase transformation FCC inside the shear band. While the phase transformation in the CoCrNi thin film is insightful and leads to superior yield strength up to ~4 GPa, parallels cannot be drawn between the thin film and bulk samples because of the inherent difference between them, namely: (1) the initial grain size in thin films is small and one of the reasons of high yield strength, (2) sputtered thin films have a strong texture which is generally not seen in bulk sample, (3) the area of the film considered in these works consisted of 60% HCP and 40% FCC phase to start with. The high density of SFs already present in the HCP phase also promotes the HCP to FCC transformation, while in the case of the bulk sample, the initial microstructure is essentially single-phase FCC. There is a need to explore these sequential FCC→HCP→FCC transformations with respect to CoCrNi related alloys in bulk samples. The limited knowledge from the thin film work can be applied and extrapolated to nanocrystalline bulk samples and the possibility, as well as conditions, of bidirectional transformations need to be investigated.

2.3. Chemical short-range order

Majority of early research assumed CCAs exhibited completely random solid solution phases where each element has an equal probability of occupying any given lattice sites [2]. Over the years, the importance of enthalpic interactions in determining phase stability at lower temperatures has been recognized. Experimental evidence demonstrates that previously considered single phase CCAs exhibit phase decomposition at intermediate temperatures, confirming that the single-phase state is a high temperature state of the alloy, metastable at room temperature through quenching from high temperature. It was also predicted that in CCAs, instead of a random distribution of elements, there are regions where an element has more preference to chemically bond with some elements than others. The deviation from the random solid solution distribution may lead to formation of nanoclusters, long-range order or short-range order. In general, nanoclustering refers to preferential segregation of like elements together locally in form of nanoprecipitates [46]. Long-range order refers to an arrangement where some elements occupy one sublattice while some occupy the other sublattice with a strict distinction between the two sublattices. Secondary precipitates with L1$_2$, B2, etc. ordered lattice structure correspond to long-range order in CCAs. On the other hand, chemical short-range order (CSRO)

occurs when an element prefers/avoids other elements as the nearest or second-nearest neighbor [47,48] CSRO is fundamentally a fluctuation in the local atomic arrangement that deviates from the random arrangement of the CCA matrix, and no distinct lattice structure is formed. CSRO can influence the SFE, deformation mechanisms and mechanical properties of CCAs which will be discussed in this section, with a focus on the CoCrNi ternary alloy.

One of the early efforts to detect CSRO in CoCrNi ternary alloy was made by F.X. Zhang et al. [49] using EXAFS measurements, where these authors observed that Ni-Cr and Co-Cr bonds had smaller Debye-Waller factors. This implied that these bonds are favorable and could lead to short-range ordering within the system. Another study by Zhang et al. [50], using energy-filtered TEM, verified that CSRO was present in the CoCrNi alloy which was homogenized at 1200 ℃ and aged at 1000 ℃, followed by furnace cooling. No such ordering was found in case of the alloy homogenized and quenched to room temperature. Similarly, CSRO was observed by Zhou et al. [48] in alloys homogenized at 1100 ℃ and recrystallization annealed at 600 and 1000 ℃. Characterizing CSRO has been a challenging task for the CCA community because of the need to acquire detailed information at the atomic scale. Experimental efforts are underway to understand CSRO in the CoCrNi system; theoretical studies also predict the formation of CSRO in this system [51–53]. Walsh et al. [52] explained bonding preferences using the magnetic interaction within the CoCrNi system that dominates the CSRO. According to their spin-polarized DFT calculations: (1) Frustration of magnetic moment in case of Cr pair make them unfavorable; (2) Anti-alignment of Co and Cr spins is preferred which agrees with the tendency to form Co-Cr pairs; and (3) Replacing Co with Ni helped in reducing the same- spin Co-Cr, hence supporting the favorable Ni-Cr bonds earlier predicted. Ding et al. [53] showed similar ordering arrangement through Monte Carlo simulations using $\Delta\delta^k_{ij}$ (i,j= Cr/Co/Ni) a parameter to quantify local chemical ordering around individual atoms in CoCrNi. Positive values of this parameter as shown in Fig. 5(a) correspond to unfavored pairs while the negative values correspond to favorable pairs. For the first nearest neighbor, $\Delta\delta^1_{Cr-Cr}$ is ~1.58, whereas $\Delta\delta^1_{Cr-Co}$ is around −0.98, and $\Delta\delta^1_{Cr-Ni}$ is bout −0.61, which agree with previous works showing an unfavorable Cr-Cr neighboring and a preference of Cr to have Co or Ni as the nearest neighbor.

The occurrence of CSRO in the CoCrNi alloy is particularly interesting and not intuitively predicted as all the three elements have similar atomic radii and show a small heat of mixing. In the same way, the equiatomic ternary CoCrNi is the stable single phase FCC material. Though no secondary phase has been detected experimentally when the alloy is conventionally cast, the possibility exists that the FCC phase could be a metastable phase. Other phases may appear at intermediate temperature during ideal equilibrium conditions as predicted by ThermoCalc (shown Fig. 5(b)). Hence, the arrangement of atoms leading to
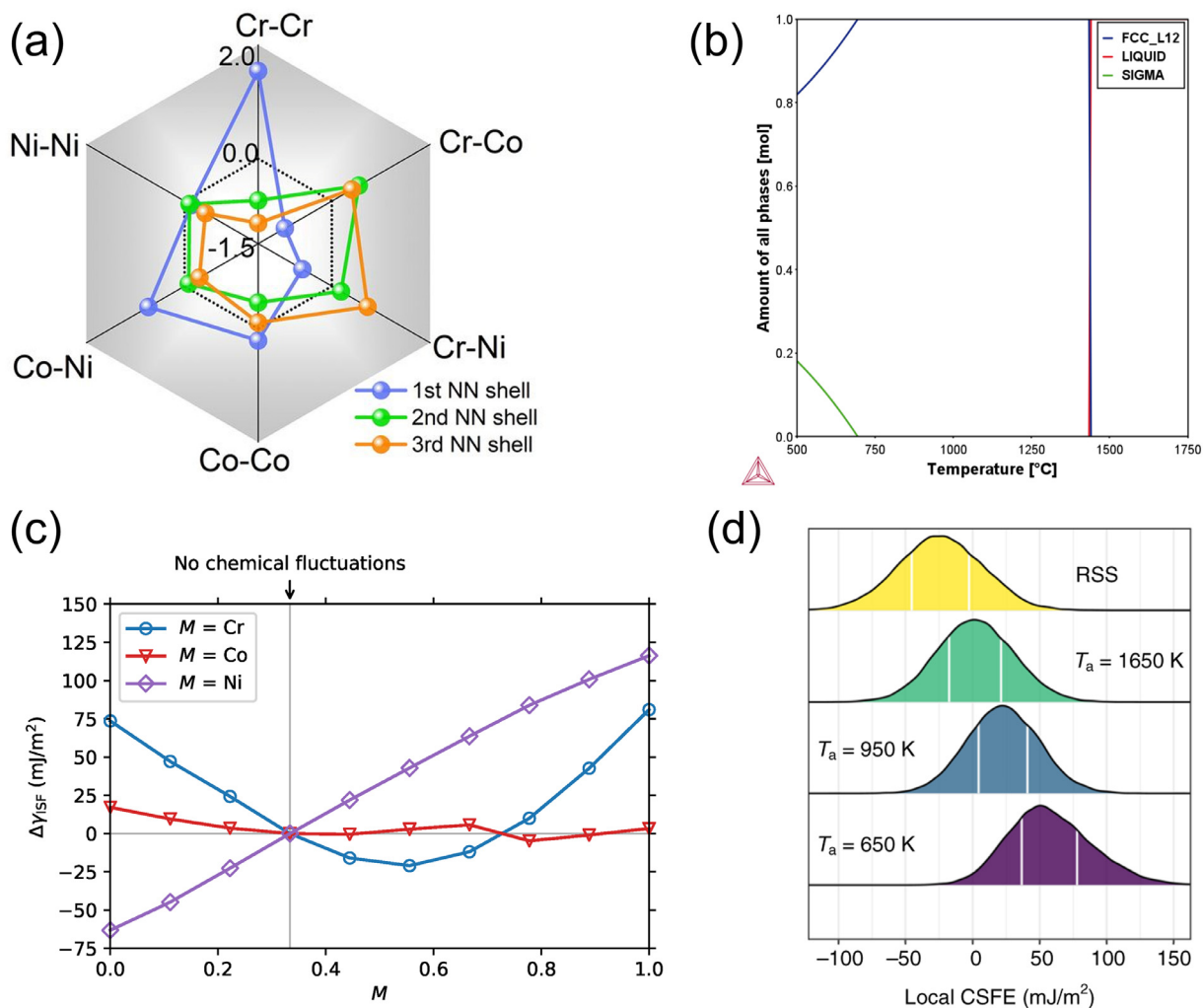
Fig. 5. (a) MC calculation parameter $\Delta\delta^k_{ij}$ for first, second and third nearest-neighbor shells [53]; (b) Phase stability map of equiatomic CoCrNi alloy calculated using ThermoCalc TCHEA5 database; (c) Variation of SFE based on the local chemical fluctuation withing the material [54]; (d) Probability density distributions of local SF energy of random solid solution (with no short-range order) and for samples annealed at 650, 950, and 1650 K, respectively (higher the temperature, lesser the ordering) [55].

CSRO could be an artifact of the potential secondary phase formation. This hypothesis needs to be backed by both experimental and theoretical studies. Though the reason behind CSRO in CoCrNi needs more investigation, several recent studies do confirm its presence in the ternary alloy, and it is important to understand the factors that can tailor the CSRO. The local chemical environment in CoCrNi as well as other CCAs is not just determined by the thermodynamically lowest energy configuration but also by the heat treatment and kinetics of thermal processing. Generally, lower annealing temperature can decrease the entropic effects and make it more favorable for the atomic pairs with lower energy to bond and hence give rise to chemical ordering within the system [55,56]. Besides the heat treatment temperature, the cooling rate could also be a deciding factor. For instance, in the work done by Zhang et al. [50], CSRO occurs in alloy that is aged, and furnace cooled. In contrast, in the study conducted by Yin et al. [57], the alloys were not slowly cooled and no CSRO was found in the CoCrNi alloy. As important as the ageing temperature is, the slow rate of furnace cooling could allow the sample to acquire the energetically favorable CSRO arrangement. Hence, the cooling kinetics of the processing could play a significant role in promoting/suppressing CSRO. More experimental evidence can further establish the connection between heat treatment temperature, cooling rate and CSRO in the CoCrNi alloy.

Such a processing-structure relationship gives opportunities to not only tailor the CSRO but also effects the SFE and deformation substructures. This kind of CSRO, if in the vicinity of SFs, will influence the SFE locally. Ikeda et al. [54] highlighted how the intrinsic SFE can vary based on the local concentration of individual elements which is depicted in Fig. 5(c). Such dependence of SFE on the local chemistry is one of the reasons for the vast difference even in the computed SFEs for the CoCrNi equiatomic ternary [25,26,28,58]. Through DFT-based MC simulations (at 0 K), Ding et al. [53] showed that there is a large distribution in the predicted SFE values which correspond to the heterogeneity in local chemical order within the sample under consideration. It was also observed that the SFE increased with increasing CSRO [50] which can be correlated to the increase in energy requirement to not just create a fault in the FCC structure but also disrupt the ordered state near it. This can further be related to the variation in computed and experimental SFEs where the calculated SFEs are generally negative while the experimental SFE was around ~22 mJ m^{-2}. The effect of temperature has already been mentioned but it is equally important to consider the incorporation of the possible short-range order while simulating or calculating the SFE. For example, Li et al. [55] showed that in their calculation the complex SFE in the case of CoCrNi as random solid solution is -24 mJ m^{-2} but with taking local chemical ordering into account the

CSFE varies from ~1.4 to ~57 mJ m^{-2} as annealing temperature varies from 1650 to 650 K as shown in Fig. 5(d).

The variation in CSRO, hence the variation in SFE, will influence a range of phenomena within the CoCrNi alloy including the deformation mechanisms, phase transformations, and defect kinetics. As mentioned earlier formation of short-range order implies extra energy expenditure for the motion of dislocations making them difficult to move. Moreover, deformation twinning and FCC→HCP phase transformation in CoCrNi is dependent on the generation of SF which can disrupt the ordering and hence cause an increase in energy. And this effect will vary throughout the sample owing to the heterogeneous nature of the ordering and SFE making it a complex competition between dislocation slip, twinning, and phase transformation. Besides the deformation mechanisms, the CSRO can also intensify the heterogeneity in inter-diffusion of vacancies and interstitials limiting their jump due to added energy barriers. CSRO will also make the grain boundary migration difficult due to the same reason. These effects will stabilize defects like vacancies, interstitials, and grain boundaries by limiting their motions, which has been exploited to develop resistance to radiation damage in the CoCrNi alloys [59].

CSRO in the CoCrNi could also affect the mechanical properties of the system. It was found that the hardness of the aged alloy with short-range order was ~0.3 GPa higher than that of the quenched alloy, while the tensile tests show an approximate 25% increase in yield strength for the alloy with SRO. Moreover, the initial work hardening rate in the aged sample is double than that of the water quenched sample. While these results indicate the potential strengthening effects of CSRO in this alloy system, a theoretical study performed by Yin et al. [57] emphasized that CSRO may not have much influence on the strength and hardness of the CoCrNi alloy, instead the strengthening effects are majorly from misfit volumes. It is difficult to conclude the effect CSRO has on mechanical properties of the CoCrNi alloy with limited experimental data. Further efforts are needed in the direction of characterizing the CSRO, verifying the predictions made by simulation and understanding the effect of CSRO on mechanical properties of CoCrNi alloy.

In summary, whereas the SFE may be at the center of all the fundamental mechanisms of the CoCrNi alloy and is conveniently generalized, it is important to understand that it can be influenced by other factors such as composition and local chemical ordering which will lead to local SFE variations within this material. Both experimental and theoretical calculations have their pros and cons, and hence should be analyzed accordingly. While the twinning and phase transformation in CoCrNi is similar to existing steels, the basic difference between CCAs and conventional alloy should be considered while drawing the comparison. Moreover, CSRO should be given special importance given its ability to change the basis of all the mechanisms. Careful control of the thermodynamics and kinetics of processing of these alloys can be useful in tuning the CSRO. Despite their complex nature, efforts need to be made towards the characterization of CSRO, both qualitatively and quantitatively, along with establishing the relationship between short-range order and mechanical properties.

3. Microstructural features and their role in modifying mechanisms

Microstructural features and atomistic mechanisms in the CoCrNi alloys are interdependent, allowing researchers to employ microstructural engineering to further enhance mechanical properties. As an example, the equiatomic CoCrNi alloy shows an excellent combination of ultimate tensile strength, ductility, and fracture toughness at micrometer level grain size, however, its yield strength at room temperature can yet be improved. In this section, we review and discuss the ways in which microstructure can be designed to affect deformation mechanisms as well as mechanical properties. Firstly, the techniques such as thermo-mechanical processing and torsional deformation processing are discussed to improve the mechanical behavior of CoCrNi alloys. More-

over, surface modification processes and grain size effects are discussed in the latter part of the section.

3.1. Gradient microstructures

One of the ways to improve the yield strength of the ternary alloy, without any composition change, is to tailor heterogeneity in microstructure in such a way that it is a composite of harder regions that give the strength and softer regions that accommodate strain, hence mitigating the strength – ductility tradeoff. In the case of the CoCrNi alloy system, the gradient does not necessarily relate to grain size but also to deformation substructures: dislocations, SFs, twins, and the HCP phase. A good portion of research related to CoCrNi is focused on achieving heterogeneous microstructure through gradients in either recrystallized/partially recrystallized grains or gradients in strain/deformation. Both approaches are discussed below.

3.1.1. Gradient in recrystallization

One of the most common techniques to achieve a gradient microstructure is subjecting the alloy to cold rolling and annealing in a way that a partially recrystallized microstructure can be obtained [60–66]. Slone et al. [67] investigated the cold-rolled CoCrNi alloy after annealing at 873 K for 1 hand 4 h which exhibited partially recrystallized structure with 39 and 76% of the volume being recrystallized respectively and the non-recrystallized structure strained the twins and dislocations produced during cold rolling. The sample annealed at 873 K for 4 h showed an increased yield strength of around 797 MPa with a uniform elongation of 19% which could be attributed to the variation in local strain along the sample as shown in Fig. 6 where the recrystallized regions deform more than the non-recrystallized ones. The recrystallized grains, being softer, can accommodate more strain and are ductile, while the non-crystallized regions, having high dislocation densities and twins, contribute to the hardening and strengthening of the material. When combined, such a heterogeneous microstructure gives the optimum combination of both strength and ductility. Moreover, such heterogenous structures also perform well under impact loading [66]. Apart from cold rolling, cryo-rolling and subsequent annealing are also potential thermo-mechanical routes for CoCrNi as the cryogenic temperature will further intensify the deformation mechanisms in the system. Along this vein, Zheng et al. [68] observed that cryo-roll deformed CoCrNi consisted of dislocation structures, nano-scale deformation twin bundles, and nano-sized grains which partially recrystallized on annealing at 973 K for 10 min, leading to a yield strength of ~1123 MPa and a uniform elongation of 31.2%.

3.1.2. Gradient in deformation structures

Another useful technique to achieve a heterogeneous microstructure for a single-phase alloy is through torsional deformation. When a CoCrNi alloy is subjected to high-pressure torsion (HPT) [69], the surface of the rod that undergoes severe torsional deformation will give a high density of twin and dislocation density while the center of the rod which is deformed the least shows a low density of deformation structures. HPT in combination with annealing [70–73] can be used to tailor grain size as well as obtain heterogeneous deformation structure. Liu et al. [69] through experimental and theoretical study described the heterogeneity induced by high-pressure torsion in the microstructure and hence the properties which are shown in Fig. 7. The optimum torsional angle for HPT that gives a good combination of strength and ductility needs to be determined. In this case for an angle of 20π, the yield tensile strength increased from 245 MPa (for initial undeformed sample) to 760 MPa while ~31% uniform elongation is maintained. Another torsional deformation process like hot swaging has been utilized for the same purpose of creating a gradient microstructure [74,75].
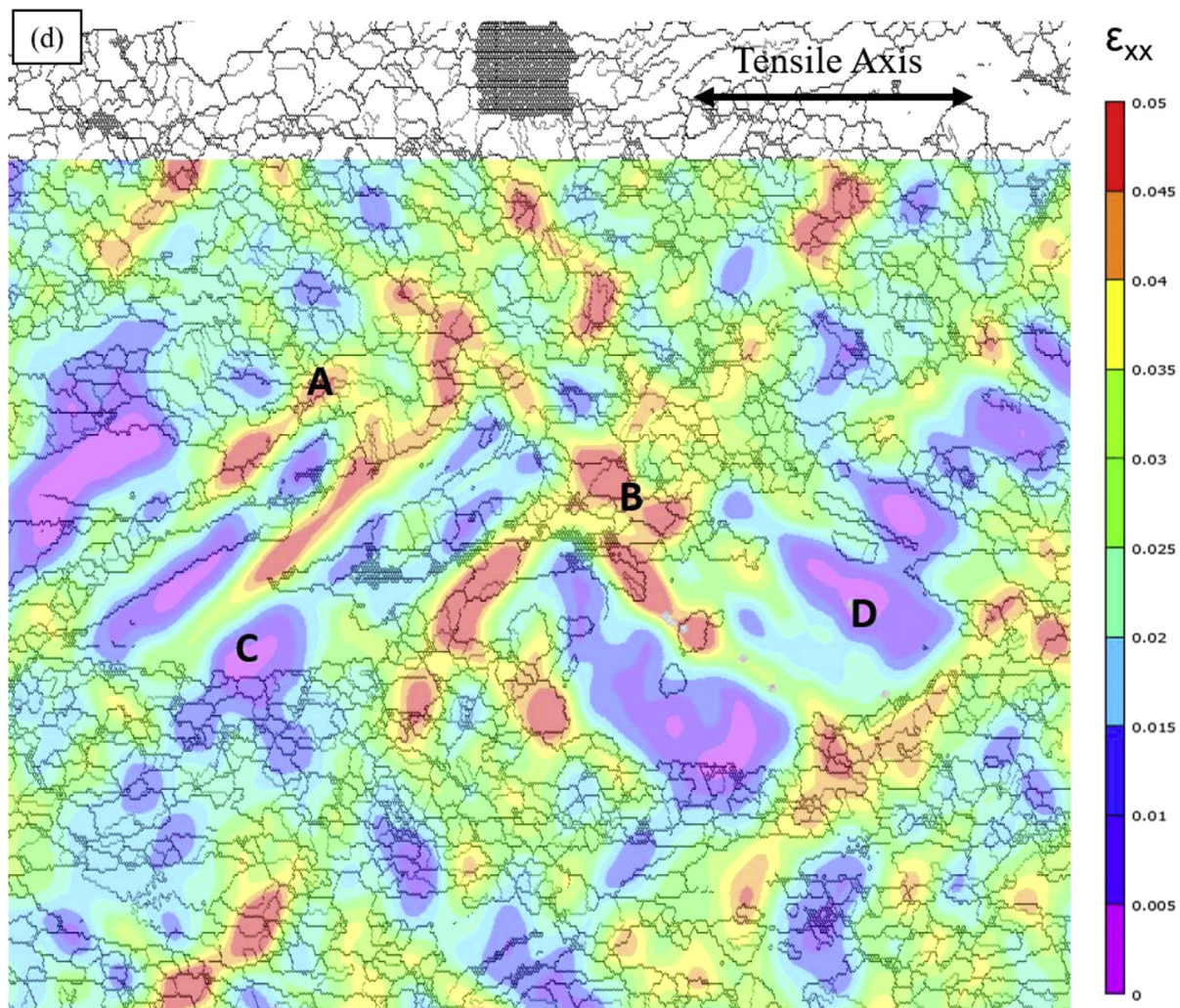
Fig. 6. Micro-digital image correlation (DIC) strain map showing variation in local strain between recrystallized (smaller grain at the top and bottom) and non-recrystallized (larger elongation grains at the center) [67].

3.2. Surface modification

Manipulating surface microstructures using severe plastic deformation (SPD) techniques such as shot peening and ultrasonic nanocrystal surface modification (UNSM) enhances, not only the mechanical properties, but also the fatigue and corrosion resistance. The SPD techniques generally form a gradient nanostructured surface to introduce residual compressive stresses that help in preventing the onset of failure [76]. The interior of the material remains relatively undeformed leading to gradual transition in grain size and strain from surface to the interior. The accumulation of geometrically necessary dislocations at the coarse-fine grain interface activates back-stress hardening [77]. These techniques have been utilized to improve strength of metallic alloys while maintaining their ductility [77–81]. For instance, UNSM processed $Fe_x(CoNi)_{90-x}Cr_{10}$ medium-entropy alloy [81] exhibited yield strength twice as much as that of as-annealed specimens. The yield strength and tensile strength of UNSM treated $Fe_{57.5}(CoNi)_{32.5}Cr_{10}$ is 528 MPa and 676 MPa respectively as compared to 223 MPa and 513 MPa of the as-annealed material. Similar observations were made for CoCrFeMnNi alloy [79] where the UNSM treatment led to enhanced strength and the loss in ductility was directly proportional to the UNSM load. Additionally, the tendency of nano-sized deformation twinning in areas closer to the surface and this effect increases with the increase in the load applied during the UNSM treatment. The CoCrNi alloy sys-

tems can show similar, potentially enhanced gradients of deformation structure and hence increased synergy between strength and ductility. Also, it is important to understand if such SPD techniques can lead to any possible phase transition within the system and how it affects the mechanical properties.

3.3. Modifying critical twinning stress by changing the grain size

Besides a favorable SFE, for twins to nucleate and grow, it is important that the stresses within the materials exceed the critical stress required to generate twinning. Since the nuclei for twins, i.e., SFs, already exist in low SFE materials, this stress mainly corresponds to the growth of twins. If the critical twinning stress is above the ultimate tensile strength, twinning will not be activated. Laplanche et al. [23] calculated the twinning stress for both equiatomic CoCrNi and CrMnFeCoNi to be 260 ± 30 MPa and 235 ± 10 MPa, respectively and emphasized that it is easier to reach the twinning stress in case of ternary alloys because of its higher yield strength and work hardening rate. It is to be noted that this calculation was done at a fixed grain size. As mentioned previously, the extent of twinning increases as the temperature decreases because the twinning stress does not vary much with temperature, whereas flow stress increases rapidly as the temperature decreases making it easier to reach the critical twinning limit at lower temperatures leading to the higher extent of twinning [20]. While twinning stress shows weak de-
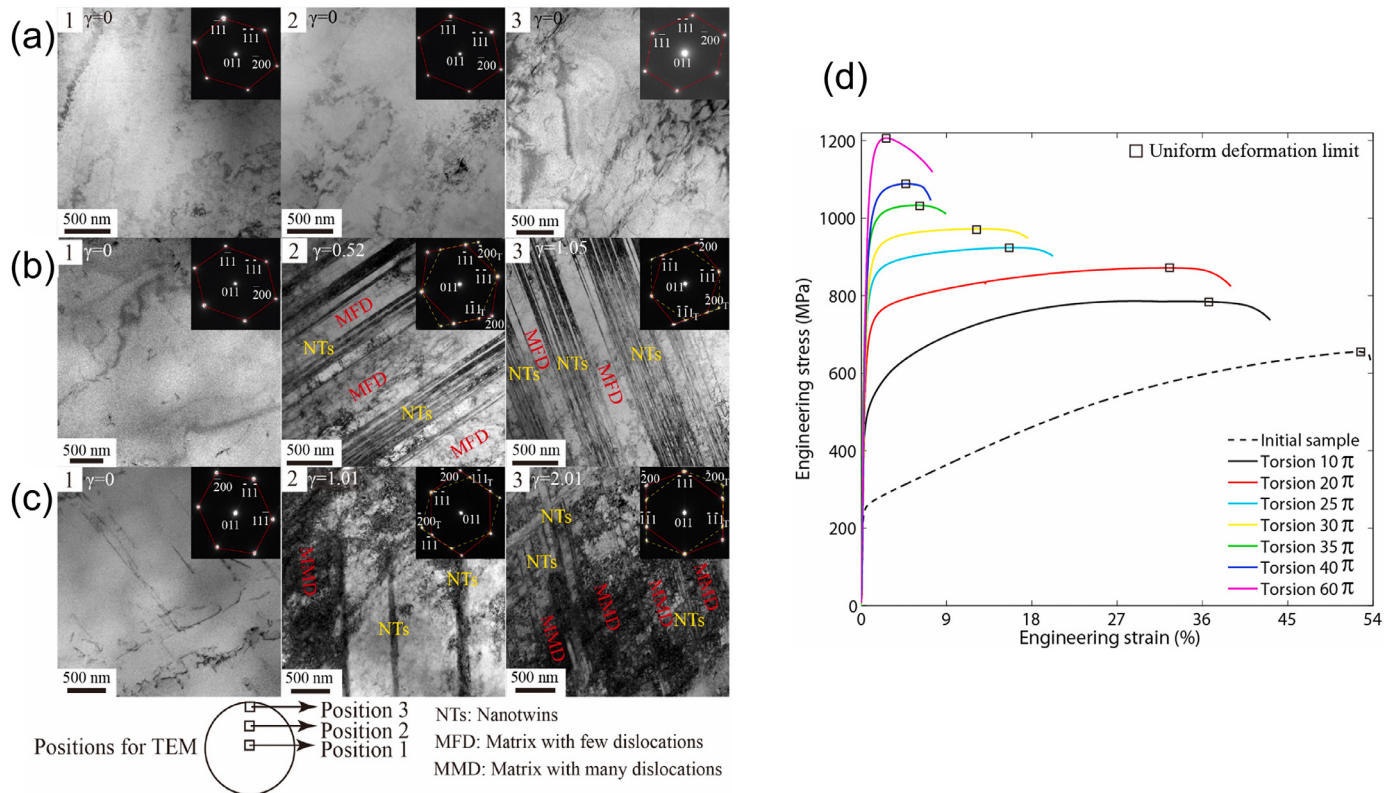
Fig. 7. TEM micrographs of (a) initial as-cast sample (b) Sample deformed via HPT at 20π torsional angle (c) Sample deformed via HPT at 40π torsional angle (d) Tensile behavior of various sample deformed at different torsional angles [69].

pendency on temperature, it can be considerably affected by grain size. For instance, in the case of TWIP steel with a composition 15Mn–2Al–2Si–0.7C (wt.%), it was found that the critical twinning stress increases with decreasing grain size [82]. This grain size-twinning stress relationship has two major implications. First, it suggests that thicker (or wider) twins will form in coarser grains while the fine grains will have thinner twins; therefore, coarse grains will be able to accommodate more plastic strain during cyclic loading. Second, in the case of broader grain size distribution, twins will be found in only some grains while the rest will contain planar slip [83]. Though no direct relationship has been established for critical twinning stress and grain size for CoCrNi alloy, there might be a possibility that similar grain size effects are also observed for CoCrNi and an optimum grain size may define critical twinning stress of CoCrNi in a way that the twins and dislocations can synergistically contribute to the mechanical performance of the CoCrNi alloy.

In summary, the presence of a gradient in the microstructure, whether through surface modification and/or in the form of grain size, the extent of recrystallization, or the density of deformation structures, can be introduced through a series of deformation processing and thermal treatments. If engineered properly, the strength-ductility tradeoff can be mitigated. Another important property to consider while subjecting these alloys to thermo-mechanical processing is their effect on the fracture toughness of the CoCrNi which is quite good in the fully recrystallized state. Further work is needed in this direction. It will be also beneficial to examine the effect of such heterogeneous microstructure on the cryogenic properties of this material.

4. Derivative systems

This section covers findings related to derivative systems which are defined as those obtained via some minor alloying addition to a base ternary system to enhance solid solution strengthening, and in some cases, precipitation strengthening as well. This section focuses on five

important alloying additions made to the CoCrNi systems: Aluminum, Titanium, Molybdenum, Tungsten, and Silicon. The influence of these elements on the phase structure and mechanical properties of the derivative alloy is discussed for specific systems as well as in the context of the overall influence of alloying additions on atomistic mechanisms on CoCrNi.

Some of the relevant properties of the base elements and alloying additions are listed in Table 1. If additional phase/s appear there could be a synergy between solid solution strengthening, precipitation strengthening, and grain boundary strengthening. In related studies, Hu et al. [84] pointed out the significance of self-diffusion activation energy (SDQ) of alloying elements which revolves around the idea that a higher drag will be imposed by the solute with a low diffusion rate which in turn will inhibit grain coarsening and vice versa. Alloying elements may also delay recrystallization leading to finer grain size. These effects are common for conventional alloys and other CCAs as well. In the case of CoCrNi, it is also important to account for the effect these alloying elements will have on the SFE, CSRO and hence deformation twinning and FCC→HCP phase transformation.

4.1. Aluminum

One of the important alloying additions that is added to the base ternary CoCrNi is Al. Al is a strong BCC phase former and due to the atomic size difference will distort the lattice. It has been shown that a single-phase FCC structure is stable with up to 7 at.% addition of Al [86]. Lattice distortion in the matrix is increased and consequently, the yield strength increases as the Al content increases from 0 to 7 at.%. Al also reduces the mass density of the alloy. Lee et al. [87] investigated the alloy with composition $Al_{7.5}CoCrNi$ which showed an additional B2 phase in the FCC phase. It was observed that the propensity for twinning was reduced in the sample. Though the effect of Al on SFE was not clear, Al led to the refinement of grains and was found to increase

Table 1

Atomic radius [85], crystal structure, and melting point [5] of constituent elements in CoCrNi based CCAs.

Elements	Cr	Co	Ni	Al	Ti	Mo	W	Si
Atomic Radii (nm)	0.12491	0.12510	0.12459	0.14317	0.14615	0.13626	0.13670	0.11530
Crystal structure	BCC	HCP	FCC	FCC	HCP	BCC	BCC	Diamond
Melting point (K)	2180	1768	1728	933	1941	2896	3695	1687

Table 2

Phase structure and tensile properties of CoCrNi alloys with Al addition (H: Homogenization, CR: Cold Rolling, A: Annealing).

Alloy	Processing steps	Phase(s) formed	Yield Strength (MPa)	Tensile Strength (MPa)	Elongation (%)	Ref.
$Al_0CoCrNi$	Arc-melting	Single-phase FCC	250.3	759.5	73.2	[86]
$Al_2CoCrNi$	H: 1000 ℃ 24 h		260.7	763.0	75.3	
$Al_4CoCrNi$	CR: 90%		281.0	771.7	73.8	
$Al_7CoCrNi$	A: 1100 ℃ 5 min		305.9	794.9	67.9	
$Al_{7.5}CoCrNi$	Arc-melting H: 1000 ℃ 24 h CR: 90% A: 900 ℃ 30 min	Single phase FCC + NiAl- rich B2 precipitate	680	1044	48	[87]
$Al_2CoCrNi$	Arc-melting	Single FCC	-	-	-	[88]
$Al_4CoCrNi$		Single FCC	219.38		>50	
$Al_8CoCrNi$		Single FCC	236.66		>50	
$Al_{16}CoCrNi$		FCC+BCC	760.52		34.57	
$Al_{22}CoCrNi$		Double BCC	1531.79		18.16	
$Al_{30}CoCrNi$		Double BCC	1765.48		10.24	
$Al_{0.3}CoCrNi$	Induction Melting H: 1200 ℃ 6 h CR: 78% A: 800 ℃ 60 min	FCC + NiAl-rich B2 + CrCo rich Sigma	945	1230	38	[89]

the critical twinning stress making it difficult for twins to nucleate. An increase of the lattice constant was observed in this case as well. A combined effect of solid solution, grain boundary, and precipitate strengthening lead to an increase in tensile strength by 53.73 MPa as compared to CoCrNi. In another study Lu et al. [88] studied $Al_xCoCrNi$ alloys and found that at low Al concentration (x < 12 at.%), the alloys had a single-phase FCC structure which evolved to a dual-phase FCC + BCC structure for 12 at.% < x < 22 at.% and to a double BCC phase structure for 22 at.% < x < 32 at.%. This observation highlights the role of Al as a BCC phase stabilizer. The yield strength increases, but at the expense of ductility, as the Al content increases which contributes to the formation of hard BCC phases. It should also be pointed out that for Al concentration greater more than 22 at.%, the alloy has a composition similar to a quaternary alloy than the ternary alloy and the results may not be directly compared to the ones with minor alloying additions. Nevertheless, the general trend observed with the Al addition involves, formation of the BCC phase above a certain Al concentration accompanied by an increase in yield strength and a decrease in elongation. While Agustianingrum et al. [86] did not observe any secondary phases below 7 at.% Al, work done by Sathiyamoorthi et al. [89] shows an FCC + B2 + σ phase for the $Al_{0.3}CoCrNi$ system. One of the basic differences in both cases lies between the processing and heat treatment of the alloy which has a significant impact on the initial microstructural conditions and phase stability. Processing details and the results obtained in the studies mentioned above are listed in Table 2.

4.2. Titanium

Another widely used alloying addition is Ti. Specifically, when Al and Ti are added to the CrCoNi system, in the right proportion, the γ' phase forms which is already known to yield excellent properties in Ni-based superalloys [90]. The γ' phase has a $L1_2$ ordered FCC structure which is generally coherent with the disordered FCC matrix and contributes to the strength of the alloy without compromising ductility. With the same understanding, Al and Ti are generally added in mutual proportions to the base CoCrNi alloy giving rise to an FCC+$L1_2$ dual-phase structure. Zhao et al. [91] studied the $(CoCrNi)_{94}Al_3Ti_3$ alloy and found two different precipitate distributions as shown in Fig. 8; one originated from the grain boundaries and precipitated in a discontinuous fashion, and the other in the interior of the grains where continuous precipitates with spherical morphologies were observed. Both types of precipitates were rich in Ni, Al, and Ti. The $(CoCrNi)_{94}Al_3Ti_3$ exhibited 750 MPa yield strength while maintaining good elongation of 45%, in contrast to a yield strength of 430 MPa in CoCrNi, a 44% increase. Another important observation made by this study is that the deformation twinning was less prevalent in the alloy with Al and Ti and that deformation was mainly dominated by SFs. While the effect of alloying on SFE was not calculated it was emphasized that the small width of the gamma phase, presence of very fine precipitates, and the anisotropy of the dislocation mobility might have impeded the nucleation of mechanical twins.

The same composition was studied by another group of researchers [92] who also observed $L1_2$ phase formation, though only continuous spherical precipitates and similar effects on mechanical properties were observed. Their study highlighted the slow coarsening rate of the precipitates when aged at 800 ℃ for various times. The precipitate particles maintained their spherical morphology and nanoscale size during all the aging time which was contributed to the small interfacial energy of these coherent precipitates and possible slow diffusion behavior in the CCAs in general. In a study of different alloy composition $(CoCrNi)_{94}Al_{1.5}Ti_{1.5}$ by Guo et al. [93] no precipitates or secondary phases were observed but twinning was found to be reduced when the alloy was subjected to two different degrees of torsion both at room temperature and 77 K. It was again correlated to the increase in critical stress for twinning and the bending effect of torsion on the twin boundary which makes the twin boundary deviate from the ideal angle eventually converting them to low angle boundaries. Slone et al. [94] also observed similar deactivation of twinning in CoCrNi based alloy with ~4.1 at.% Al, 2.3 at.% Ti and 0.9 at.% Nb; through DFT calculations Slone showed that the Al-Al bonds are highly unfavorable in the HCP phase and this could be the reason shearing via partial dislocation is prevented as they lead to a formation of local HCP stacking, and instead the glide of perfect a/2 <110> dislocations is preferred. Since partial dislocation shearing, i.e., formation of SFs is a precursor to twin formation, twinning will be re-
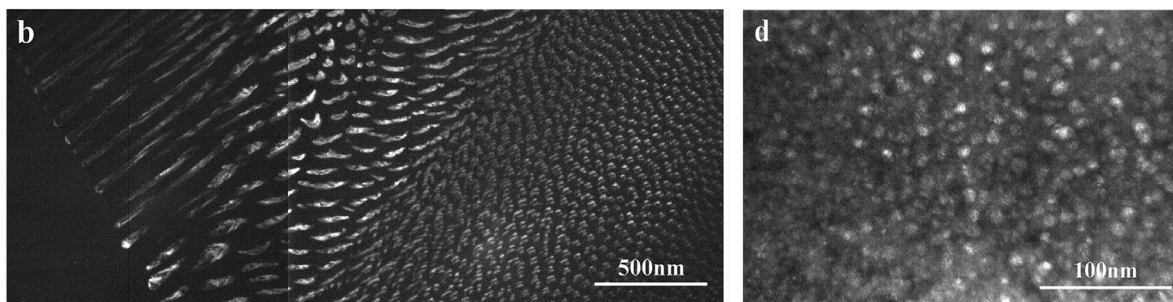
Fig. 8. Dark-field TEM micrographs showing continuous precipitation (on the left) and discontinuous precipitation (on the right) in the $(CoCrNi)_{94}Al_3Ti_3$ [91].

duced as well due to the addition of Al and Ti. The addition of these two elements introduces a trade-off between dislocations and twinning but the formation of coherent $L1_2$ precipitates has a positive effect on the strength with a slight loss in ductility.

Ti when added with C [95] was found to change the morphology of the as-cast specimen from columnar to equiaxed even in the regions closer to mold. It is believed that though Ti and C do not form a carbide, they may be rejected into the liquid ahead of the solid-liquid interface, causing constitutional supercooling and destabilizing the planar solidification front. The $(CoCrNi)_{99.2}Ti_{0.4}C_{0.4}$ system showed the finest grain size as well as mechanical properties that exceeded those of the base ternary CoCrNi.

4.3. Molybdenum

Mo, besides inducing precipitation and solid solution strengthening within the CoCrNi matrix [96–100], has a very significant effect on the grain growth kinetics of the alloy it is added to. Mo has high self-diffusion activation energy which intensifies the solution drag effect and inhibits the grain growth which leads to an added grain boundary strengthening in the CoCrNi-Mo alloys [84]. Depending on the Mo concentration and processing conditions, Mo tends to form a sigma phase which is rich in both Mo and Cr. Chang et al. [96] showed that it was only after 5 at.% Mo that the sigma phase could be seen in the $CoCrNiMo_x$ alloys. Since the sigma phase is hard and brittle, it may contribute to strength but has a detrimental effect on the ductility of the alloy. That is why in this work best strength-ductility synergy was attained for the $CoCrNiMo_3$ alloy. Li et al. [98] observed a similar trend for $CoCrNiMo_x$ (x = 0, 0.1, and 0.2 in molar ratio) where they found grain size decreased and the sigma phase content increased with increasing Mo content. Through DFT calculations (at 0 K) it was found that SFE of $CoCrNiMo_3$ was similar to that of CoCrNi and both, twinning and dislocations, contribute to the deformation. In another study by Chang et al. [97], it was observed that for an alloy with composition $(CoCrNi)_{93}Mo_7$, there was a difference in how precipitates were distributed in as cast + cold-rolled + annealed samples, where one region is rich in precipitates while the other is depleted of it, as compared to the uniform grain boundary precipitation in case of homogenized + cold-rolled + annealed samples. The as-cast sample showed better strength and ductility than the homogenized one because the presence of brittle precipitates at the grain boundaries (in the case of homogenized samples) lead to the weakening of the interface and hence an early onset of instability. Such a heterogeneous precipitation behavior highlights the importance of each processing step in microstructural evolution and mechanical properties. Table 3 lists the results from published studies on CoCrNi-Mo alloys.

4.4. Tungsten

Similar to Mo, W also has high self-diffusion activation energy which leads to slow grain growth kinetics which adds to strengthening mechanisms caused by large lattice and modulus mismatch of W with Cr, Co,

and Ni. Guo et al. [93] observed that that as the W content increased, the recrystallization retarded, and grain size decreased which is intuitive. With additions of up to 3 at.% W, no secondary phases were observed. They calculated the grain growth activation energy which was 301.0 ± 7.1 kJ/mol, 314.3 ± 5.8 kJ/mol, and 393.3 ± 9.2 kJ/mol for 0 at.% W, 1 at.% W, and 3 at.% W respectively highlight the solute drag effect of W leading to slower grain growth. Though this work did not calculate the effect of W on SFE of CoCrNi, using the previous literature, it predicted that SFE will increase with W doping. This claim warrants further theoretical and experimental study. Wu et al. [101] also studied CoCrNi-W alloy with 3, 6, and 9 at.% W doping. Though they did not find any secondary phase with 3at.% W, the other two compositions had W- rich secondary phases which agrees with ThermoCalc predictions showing the evolution of the secondary phase at ~4 at.% W. The mechanical testing showed an increase in both strength and ductility of CoCrNi-3 at.% W as the temperature changed from 293 to 77 K and it was also observed that deformation twinning was prevalent at 77 K while at 293 K, only dislocation glide and cross-slip dominated the deformation. Hence W leads to solid solution and grain boundary strengthening in the alloys. The mechanical behavior of W alloyed CoCrNi CCAs is listed in Table 4. In a sense, the prediction of increased SFE with W doping [102] aligns with the dominating presence of cross-slip at room temperature in the work by Wu et al. [101] as the width of SFs decreases with increasing SFE making cross-slip easier but this hypothesis needs to be backed by relevant data to make it more reliable.

4.5. Silicon

Si is another alloying element that has maintained the strength-ductility synergy when added to the CoCrNi ternary. In the case of TWIP steel, Si was found to lower critical twinning stress and SFE, hence promoting higher ductility and work hardening [103]. Chang et al. [104] investigated the $CoCrNiSi_x$ alloy for x = 0.1, 0.2 and 0.3. It should be noted that x here is the molar ratio and not the atomic percent. These authors observed that for homogenized, cold-rolled, and annealed samples, Si promotes recrystallization (that is contrary to other alloying elements retarding it) which eventually leads to an increase in grain size with increasing Si content ruling out the possibility of grain boundary strengthening. Furthermore, multiple twins were observed in $CoCrNiSi_{0.2}$ and $CoCrNiSi_{0.3}$, with the twin volume fraction increasing with the increase in Si. Additionally, for $CoCrNiSi_{0.3}$, an HCP phase was observed at a strain value of 65%. The enhanced twinning and FCC→HCP phase transformation indicate towards a low SFE and through thermodynamic calculations, the effective SFEs of $CoCrNiSi_x$ (x = 0, 0.1, 0.2) were calculated to be 17.4, 12.9, and 7.6 mJ m^{-2} This calculation illustrates the positive effect of Si in lowering the SFE of CoCrNi alloys. In another study by Liu et al. [105] for the same alloy compositions showed the addition of Si to base ternary maintains the SFE. They also found two types of precipitate formation for the $CoCrNiSi_{0.3}$ alloy, which in this case was σ-type tetragonal-structure phase enriched with Cr and Si, and the other one was enriched with Cr with an unidentified crystal struc-

Table 3

Phase structure and tensile properties of CoCrNi alloys with Mo addition (H: Homogenization, CR: Cold Rolling, A: Annealing).

Alloy	Processing steps	Phase(s) formed	Yield Strength (MPa)	Tensile Strength (MPa)88u	Elongation (%)	Ref.
CoCrNi-3wt%Mo	Arc melting H: 1100 ℃ 48 h CR: 88% A: (1) 850 ℃ 2 h (2) 900 ℃ 2 h	Single FCC	(1)535 (2)435	(1)963 (2)901	(1)73 (2)74	[84]
$(CoCrNi)_{99}Mo_1$ $(CoCrNi)_{97}Mo_3$ $(CoCrNi)_{95}Mo_5$	Arc melting H: 1200 ℃ 4 h CR: 66% A: 900 ℃ 1 h	Single FCC Single FCC FCC+ CrMo-rich Sigma phase	412 475 528	914 983 1026	63 69 47	[96]
$CoCrNiAl_{0.1}Mo_{0.1}$	Arc melting H: 1200 ℃ 2 h CR: 80% A: 725 ℃ 1 h	FCC + Cr-rich μ precipitates	1100	1304	22	[100]
$(CoCrNi)_{93}Mo_7$	Arc melting H: 1200 ℃ 5 h CR: 60% A: 900 ℃ 1 h	FCC+ CrMo-rich Sigma precipitates	560	1135	35	[97]

Table 4

Phase structure and tensile properties of CoCrNi alloys with W addition (H: Homogenization, WR: Warm Rolling, CR: Cold Rolling, A: Annealing).

Alloy	Processing steps	Phase(s) formed	Yield Strength (MPa)	Tensile Strength (MPa)	Elongation (%)	Ref.
$(CoCrNi)_{99}W_1$	Arc melting H: 1200 ℃ 1 h WR: 70% at 500 ℃ A: 900 ℃ 60 min	Single-phase FCC	398	857	62	[102]
$(CoCrNi)_{97}W_3$			484	943	52	
$(CoCrNi)_{97}W_3$	Arc melting H: 1200 ℃ 24 h CR: 90% A: 800 ℃ 1 h	Single-phase FCC	~1000 MPa	~1300 MPa	~45	[101]

Table 5

Phase structure and tensile properties of CoCrNi alloys with Si addition (H: Homogenization, CR: Cold Rolling, A: Annealing).

Alloy	Processing steps	Phase(s) formed	Yield Strength (MPa)	Tensile Strength (MPa)	Elongation (%)	Ref.
$CoCrNiSi_{0.1}$	Arc melting H: 1100 ℃ 5 h CR: 90% A: 900 ℃ 1 h	Single FCC *Note: FCC To HCP transition takes place during tensile testing in $CoCrNiSi_{0.2}$ and $CoCrNiSi_{0.3}$*	-	856	75	[104]
$CoCrNiSi_{0.2}$				926	86	
$CoCrNiSi_{0.3}$				950	92	
$CoCrNiSi_{0.2}$	Arc melting H: 1200 ℃ 2 h CR: 70% A: 800 ℃ 1 h	Single FCC	599	1032	50.5	[105]
$CoCrNiSi_{0.3}$		FCC + CrSi-rich Sigma type phase + Cr-rich unidentified phase	899	1285	15	
$Si_{0.3}CoCrNi$ $Si_{0.4}CoCrNi$	Arc melting only	Dual-phase FCC	-	-	-	[106]

ture. It is expected that the difference in annealing temperature in the above two studies might have been responsible for different phase formation at higher Si content, but it can be conveniently said that Si does not seem to increase the SFE of the CoCrNi alloy. In another study of the as-cast $CoCrNiSi_x$ (x = 0.1, 0.2, 0.3 and 0.4) [106], significant grain refinement and another FCC phase was observed for $CoCrNiSi_{0.3}$ and $CoCrNiSi_{0.4}$. This phase, rich in Si and depleted in Co, contributed to the hardness and yield strength of the as-cast alloys. The findings from the study of CoCrNi doped with Si are listed in Table 5.

To sum up, the addition of an alloying element to exploit various strengthening mechanisms like solid solution strengthening, precipitation strengthening, GB strengthening, etc. definitely helps in enhancing the properties of the base CoCrNi ternary alloy. It will also be more productive if alloy design concepts can be applied while tuning the composition. While few efforts are being made to understand how SFE changes with the minor addition of other elements, another area that still needs to be explored is the effect of alloying on the short-range order of the CoCrNi alloys. Even the minor addition distorts the lattice as has been observed in many works, it can be expected that it will also disturb the neighboring arrangement within the system and hence short-range order. It will be insightful if the effect of alloying on the SFE and short-range order be studied and correlated.

5. Comparison of CoCrNi CCAs with conventional FCC alloys

While the properties shown by these CCAs are remarkable, other 3d-transition metal alloys exhibit similar behavior at low temperatures. Before the discovery of CCAs, various alloys including cryogenic steels and Ni-Co based superalloys have been known for their cryogenic performances [107–121]. The compositions of some of these alloys are listed

Table 6

Composition (in wt%) of MP35N, MP159 and AEREX 350 alloys [125].

Alloy	Co	Ni	Cr	Mo	Al	Ti	Nb	Ta	W	Fe	C	B
MP35N	35	35	20	10	-	<1	-	-	-	<1	<0.02	<0.02
MP159	35.5	25.5	19	7	0.2	3.2	0.5	-	-	9	<0.02	<0.02
AEREX 350	25	44.5	17	3	1	2.2	1.2	4	2	<0.01	<0.02	<0.02

in Table 6 and Appendix A. Among these alloys, MP35N alloy exploits the FCC→HCP martensitic phase transition, which is similar to that in CoCrNi alloy, to display excellent mechanical properties. For instance, cold worked and unaged MP35N alloy has shown tensile strength of up to 2.41 GPa with a tensile elongation of 42% at 77 K [113]. MP35N also exhibits remarkable corrosion resistance and has applications as a conducting wire in biomedical devices [122] as well as reinforcement material for high field pulsed magnets [20]. MP35N was limited by its maximum service temperature making them unsuitable for temperatures higher than 573 K and hence a new alloy MP159 with more alloying addition to the base Co-Ni-Cr matrix was developed. The additions of Al, Ti, and Nb elements into the matrix can lead to the formation of $Ni_3(Al,Ti)$ γ' phase after suitable annealing treatment [123]. Both the MP alloys exhibit low stacking fault energy due to a high content of Co which facilitates the formation of deformation twinning as explained in Section 2.1. This deformation twinning can positively contribute to strain hardening and lead to strengthening to these alloys. Another member of this family is the AEREX350 alloy, which besides showing a γ' phase in aged material may also show and η phase with D024 structure may appear at grain boundaries on high temperature aging [124]. Both of the phases contribute to the strain-hardening of the alloy and it was also found that cold working prior to aging can be used to alter relative nucleation and growth kinetics of both the γ' and η phase to ensure uniform distribution and enhance the mechanical properties [114].

It is clear that alloys showing excellent mechanical properties at temperatures as low as 77 K have been developed as early as 1980s and have found many suitable applications ranging aerospace industry to orthopedic implants. With such similar composition of the MP alloys and the equiatomic CoCrNi ternary, it is important to take cues from the work already done in these materials to advance research in the CCAs.

While the basic features of twins, slip and FCC to HCP phase transition remain the same, the most prominent difference between conventional FCC alloys and CCAs is the compositional complexity in the latter. This complex compositional landscape and a highly distorted lattice leads to non-uniform interactions between the atoms and deformation structures like twins, SFs and dislocations. Unlike conventional alloys, bonds will not be uniform in the case of the base CoCrNi equiatomic ternary and other CCAs, thus, some bonds will be harder or easier to break than others. Such variation will result in non-uniform dissociation of Shockley partials and hence the local variation in SFE values. Smith et al. [126] investigated the equiatomic CrMnFeCoNi alloy and found that there was a large variation in dissociation distances where the mean SF width was 4.82 nm with a standard deviation of 1.93 nm. Using computational methods, it was also shown that at several sites, the local SFE was negative while the average SFE was positive. Shih et al. [127] also pointed out the high solute-dislocation interactions in CCAs which should be taken into consideration while experimentally calculating SFE. Using the Ni-Co model, Shih et al. [127] demonstrated the presence of an additional resistance force due to the interaction of dislocations with the large solute concentration in the alloy, which balances the forces in such a way that the equilibrium separation distance between partial dislocation remains finite even at zero or negative SFE values. Even with limited work in this direction, it can be emphasized that the value of SFE should not be taken as a single global value for CoCrNi and other CCAs. The connection between compositional complexity and the local SFE needs to be further explored. Another reason

for such a difference between calculated and experimental SFE values can be the presence of local chemical order in these alloys. It should also be noted that some of the fundamental mechanisms like chemical short-range ordering which are currently very prominent in the field of CCAs might not have been considered when studying the conventional alloys. The current and future study in the CoCrNi based alloys can be an advancement of what is already known as well as filling any gaps in the understanding of CoCrNi based alloys.

6. Conclusion and future opportunities

The equiatomic CoCrNi ternary and related alloys represent a model for a scientifically interesting and technologically promising CCA system; not surprisingly there have been numerous studies published on this family of systems. Similar and yet different from TWIP/TRIP steels, CoCrNi alloys have the potential to be used as a structural material for low-temperature applications. The compositional complexity, the range of deformation structures, phase transformation, and short-range order in the CoCrNi system opens a broad range of opportunities to tailor and engineer the processing-microstructure-properties relationship. Current research in this alloy system has been insightful and mainly focused on enhancing tensile properties, i.e., a good combination of yield strength, tensile strength, and ductility, through various thermo-mechanical processing and alloying additions. Moreover, research into deformation mechanisms suggest that indeed, the compositional complexity of these systems does influence the underlying deformation mechanisms. For example, the presence of an additional resistance force due to the interaction of dislocations with the large solute concentration in the alloy[127], which balances the forces in such a way that the equilibrium separation distance between partial dislocation remains finite even at zero or negative SFE values. Although results suggest that SFE plays a key role in the deformation of CoCrNi alloys, it is important to understand that it can be influenced by other factors such as composition and local chemical ordering which will lead to local SFE variations within this material.

As the research in the CoCrNi CCAs progresses, it is important to look into other important properties like fracture toughness and fatigue which are frequently overlooked in current research. Furthermore, investigating all these properties at the cryogenic temperature will be crucial in establish this alloy as potential candidate for cryogenic applications. With the increasing focus on CSRO, it will be important to establish an in-depth understanding of why ordering occurs and if the FCC phase is stable or metastable. It will also be beneficial to understand how the modification in processing (heat treatment temperature and cooling kinetics) affects the occurrence of CSRO and if such ordering has any effect on the mechanical properties at the bulk level, or that it is it just at the micro/nano-level. Reversible phase transformation from HCP to FCC needs to be further explored. The basic concepts inspired by the conventional alloys need to be modified to consider the compositional complexity in the CoCrNi system and the possibility of CSRO within the system. This will also help in bridging the gap between the experimental and computational efforts. Furthermore, alloy design strategies can be used to modify the derivative systems and their processing to optimize the material performance of CCAs.

Declaration of Competing Interest

The authors declare that they have no known competing financial interests or personal relationships that could have influenced this paper.

Acknowledgment

Appendix

Appendix Table A: Composition of Co-Cr-Ni based metals and superalloys.

Alloy	Co	Cr	Ni	Mo	Si	Mn	Fe	Al	Ti	W
Elgiloy [128]	39–41	19–21	14–16	6–8%	<1.2	1.5–2.5	Balance	-	-	-
HS 188 [129]	Balance	20–24	20–24	-	0.2–0.5	<1.25	<3	-	-	13–16
X-40 [130]	Balance	24.5–26.5	9.5–11.5	-	<1	<1	<2	-	-	7–8%
Haynes C263 [131]	20	20	52	6	0.2	0.4	<0.7	<0.6	<2.4	-
MAR-M 432 [132]	20	15.5	Balance					2.8	4.3	3
Nimonic 105 [133]	18–22	14–15.7	Balance	4.5–5.5	<1	<1	<1	4.5–4.9	0.9–1.5	
Udimet 500 [134]	16.5	17.5	53	4	-	-	4	2.9	3.9	-
Udimet 700 [135]	18.5	15.1	53	5	-	-	<1	4.3	3.4	-
IN 939 [136]	18–20	22-23	Balance		0.5	0.5		1.00–3.00	3–4.5	1–3.0
Nimonic 90 [137]	15–21	18–21	Balance	-	1	1	1.5	1–2.0	2–3.0	-
Nimonic 115 [138]	13–15.5	14–16	54	3–5.0	1	1	1	4.5–5.5	3.5–4.5	
Nimonic PK33 [139]	12–16.0	16–20	54	5–9.0	0.5	0.5	1	1.7–2.5	1.5–3	
Inconel 617 [140]	10–15.0	20–24	55 min	8–10.0	<1	<1	<3	0.8–1.5	<0.6	-
Rene 41 [141]	10–12.0	18–20.0	Balance	9–10.5	<0.5	<0.1	<5	<1.8	<3.3	-

References

[1] B. Cantor, I.T.H. Chang, P. Knight, A.J.B. Vincent, Microstructural development in equiatomic multicomponent alloys, Mater. Sci. Eng. A 375–377 (2004) 213–218, doi:10.1016/J.MSEA.2003.10.257.

[2] J.W. Yeh, S.K. Chen, S.J. Lin, J.Y. Gan, T.S. Chin, T.T. Shun, C.H. Tsau, S.Y. Chang, Nanostructured high-entropy alloys with multiple principal elements: novel alloy design concepts and outcomes, Adv. Eng. Mater. 6 (2004) 299–303, doi:10.1002/ADEM.200300567.

[3] S. Gorsse, D.B. Miracle, O.N. Senkov, Mapping the world of complex concentrated alloys, Acta Mater. 135 (2017) 177–187, doi:10.1016/J.ACTAMAT.2017.06.027.

[4] E.P. George, D. Raabe, R.O. Ritchie, High-entropy alloys, Nat. Rev. Mater. 4 (2019) 515–534 2019 4:8, doi:10.1038/s41578-019-0121-4.

[5] D.B. Miracle, O.N. Senkov, A critical review of high entropy alloys and related concepts, Acta Mater. 122 (2017) 448–511, doi:10.1016/j.actamat.2016.08.081.

[6] B.E. MacDonald, Z. Fu, B. Zheng, W. Chen, Y. Lin, F. Chen, L. Zhang, J. Ivanisenko, Y. Zhou, H. Hahn, E.J. Lavernia, Recent progress in high entropy alloy research, JOM 69 (2017) 2024–2031 2019 10:1, doi:10.1007/S11837-017-2484-6.

[7] D.B. Miracle, High entropy alloys as a bold step forward in alloy development, Nat. Commun. 10 (2019) 1–3 2019 10:1, doi:10.1038/s41467-019-09700-1.

[8] E.P. George, W.A. Curtin, C.C. Tasan, High entropy alloys: a focused review of mechanical properties and deformation mechanisms, Acta Mater. 188 (2020) 435–474, doi:10.1016/J.ACTAMAT.2019.12.015.

[9] B. Cantor, Multicomponent high-entropy Cantor alloys, Prog. Mater. Sci. 120 (2021) 100754, doi:10.1016/J.PMATSCI.2020.100754.

[10] A.J.B. Vincent, A Study of Three Multicomponent Alloys, University of Sussex Library, 1981 Part II Thesisn.d..

[11] B. Gludovatz, A. Hohenwarter, D. Catoor, E.H. Chang, E.P. George, R.O. Ritchie, A fracture-resistant high-entropy alloy for cryogenic applications, Science 345 (2014) 1153–1158 (1979), doi:10.1126/SCIENCE.1254581.

[12] F. Otto, A. Dlouhý, C. Somsen, H. Bei, G. Eggeler, E.P. George, The influences of temperature and microstructure on the tensile properties of a CoCrFeMnNi high-entropy alloy, Acta Mater. 61 (2013) 5743–5755, doi:10.1016/J.ACTAMAT.2013.06.018.

[13] Z. Wu, H. Bei, F. Otto, G.M. Pharr, E.P. George, Recovery, recrystallization, grain growth and phase stability of a family of FCC-structured multi-component equiatomic solid solution alloys, Intermetallics 46 (2014) 131–140 (Barking), doi:10.1016/J.INTERMET.2013.10.024.

[14] Z. Wu, H. Bei, G.M. Pharr, E.P. George, Temperature dependence of the mechanical properties of equiatomic solid solution alloys with face-centered cubic crystal structures, Acta Mater. 81 (2014) 428–441, doi:10.1016/j.actamat.2014.08.026.

[15] B. Gludovatz, A. Hohenwarter, K.V.S. Thurston, H. Bei, Z. Wu, E.P. George, R.O. Ritchie, Exceptional damage-tolerance of a medium-entropy alloy CrCoNi at cryogenic temperatures, Nat. Commun. 7 (2016) 1–8 2016 7:1, doi:10.1038/ncomms10602.

[16] F.G. Coury, K.D. Clarke, C.S. Kiminami, M.J. Kaufman, A.J. Clarke, High throughput discovery and design of strong multicomponent metallic solid solutions, Sci. Rep. 8 (2018) 1–10 2018 8:1, doi:10.1038/s41598-018-26830-6.

[17] C. Varvenne, A. Luque, W.A. Curtin, Theory of strengthening in FCC high entropy alloys, Acta Mater. 118 (2016) 164–176, doi:10.1016/J.ACTAMAT.2016.07.040.

[18] H.S. Oh, S.J. Kim, K. Odbadrakh, W.H. Ryu, K.N. Yoon, S. Mu, F. Körmann, Y. Ikeda, C.C. Tasan, D. Raabe, T. Egami, E.S. Park, Engineering atomic-level complexity in high-entropy and complex concentrated alloys, Nat. Commun. 10 (2019) 1–8 2019 10:1, doi:10.1038/s41467-019-10012-7.

[19] D.T. Pierce, J.A. Jiménez, J. Bentley, D. Raabe, J.E. Wittig, The influence of stacking fault energy on the microstructural and strain-hardening evolution of Fe–Mn–Al–Si steels during tensile deformation, Acta Mater. 100 (2015) 178–190, doi:10.1016/J.ACTAMAT.2015.08.030.

[20] S. Curtze, V.T. Kuokkala, Dependence of tensile deformation behavior of TWIP steels on stacking fault energy, temperature and strain rate, Acta Mater. 58 (2010) 5129–5141, doi:10.1016/J.ACTAMAT.2010.05.049.

[21] Y. Zhao, T. Yang, B. Han, J. Luan, D. Chen, W. Kai, C.T. Liu, J. Jung Kai, Exceptional nanostructure stability and its origins in the CoCrNi-based precipitation-strengthened medium-entropy alloy, Mater. Res. Lett. 7 (2019) 152–158, doi:10.1080/21663831.2019.1568315.

[22] Z. Zhang, H. Sheng, Z. Wang, B. Gludovatz, Z. Zhang, E.P. George, Q. Yu, S.X. Mao, R.O. Ritchie, Dislocation mechanisms and 3D twin architectures generate exceptional strength-ductility-toughness combination in CrCoNi medium-entropy alloy, Nat. Commun. 8 (2017) 1–8 2017 8:1, doi:10.1038/ncomms14390.

[23] G. Laplanche, A. Kostka, C. Reinhart, J. Hunfeld, G. Eggeler, E.P. George, Reasons for the superior mechanical properties of medium-entropy CrCoNi compared to high-entropy CrMnFeCoNi, Acta Mater. 128 (2017) 292–303, doi:10.1016/j.actamat.2017.02.036.

[24] Y. Deng, C.C. Tasan, K.G. Pradeep, H. Springer, A. Kostka, D. Raabe, Design of a twinning-induced plasticity high entropy alloy, Acta Mater. 94 (2015) 124–133, doi:10.1016/J.ACTAMAT.2015.04.014.

[25] S.F. Liu, Y. Wu, H.T. Wang, J.Y. He, J.B. Liu, C.X. Chen, X.J. Liu, H. Wang, Z.P. Lu, Stacking fault energy of face-centered-cubic high entropy alloys, Intermetallics 93 (2018) 269–273 (Barking), doi:10.1016/J.INTERMET.2017.10.004.

[26] C. Niu, C.R. LaRosa, J. Miao, M.J. Mills, M. Ghazisaeidi, Magnetically-driven phase transformation strengthening in high entropy alloys, Nat. Commun. 9 (2018) 1–9 2018 9:1, doi:10.1038/s41467-018-03846-0.

[27] S. Ogata, J. Li, S. Yip, Ideal pure shear strength of aluminum and copper, Science 298 (2002) 807–811 (1979), doi:10.1126/SCIENCE.1076652.

[28] Y.H. Zhang, Y. Zhuang, A. Hu, J.J. Kai, C.T. Liu, The origin of negative stacking fault energies and nano-twin formation in face-centered cubic high entropy alloys, Scr. Mater. 130 (2017) 96–99, doi:10.1016/J.SCRIPTAMAT.2016.11.014.

[29] T.L. Achmad, W. Fu, H. Chen, C. Zhang, Z.G. Yang, First-principles calculations of generalized-stacking-fault-energy of Co-based alloys, Comput. Mater. Sci. 121 (2016) 86–96, doi:10.1016/J.COMMATSCI.2016.04.031.

[30] L. Vitos, J.O. Nilsson, B. Johansson, Alloying effects on the stacking fault energy in austenitic stainless steels from first-principles theory, Acta Mater. 54 (2006) 3821–3826, doi:10.1016/J.ACTAMAT.2006.04.013.

[31] G.B. Olson, M. Cohen, A general mechanism of martensitic nucleation: part I. General concepts and the FCC → HCP transformation, Metall. Trans. A 7 (1976) 1897–1904 1976 7:12, doi:10.1007/BF02659822.

[32] H. He, M. Naeem, F. Zhang, Y. Zhao, S. Harjo, T. Kawasaki, B. Wang, X. Wu, S. Lan, Z. Wu, W. Yin, Y. Wu, Z. Lu, J.J. Kai, C.T. Liu, X.L. Wang, Stacking fault driven phase transformation in CrCoNi medium entropy alloy, Nano Lett. 21 (2021) 1419–1426, doi:10.1021/ACS.NANOLETT.0C04244.

[33] G.B. Olson, M. Azrin, Transformation behavior of TRIP steels, Metall. Trans. A 9 (1978) 713–721, doi:10.1007/BF02659928.

[34] Z. Li, C.C. Tasan, K.G. Pradeep, D. Raabe, A TRIP-assisted dual-phase high-entropy alloy: grain size and phase fraction effects on deformation behavior, Acta Mater. 131 (2017) 323–335, doi:10.1016/J.ACTAMAT.2017.03.069.

[35] Z. Li, K.G. Pradeep, Y. Deng, D. Raabe, C.C. Tasan, Metastable high-entropy dual-phase alloys overcome the strength–ductility trade-off, Nature 534 (2016) 227–230 2016 534:7606, doi:10.1038/nature17981.

[36] W. Lu, C.H. Liebscher, G. Dehm, D. Raabe, Z. Li, W. Lu, C.H. Liebscher, G. Dehm, D. Raabe, Z. Li, Bidirectional transformation enables hierarchical nanolaminate dual-phase high-entropy alloys, Adv. Mater. 30 (2018) 1804727, doi:10.1002/ADMA.201804727.

[37] Z.F. He, N. Jia, D. Ma, H.L. Yan, Z.M. Li, D. Raabe, Joint contribution of transformation and twinning to the high strength-ductility combination of a FeMnCoCr high entropy alloy at cryogenic temperatures, Mater. Sci. Eng. A 759 (2019) 437–447, doi:10.1016/J.MSEA.2019.05.057.

[38] F. Zhang, H. Lou, B. Cheng, Z. Zeng, Q. Zeng, High-pressure induced phase transitions in high-entropy alloys: a review, Entropy 21 (2019) 239 2019, Vol. 21, Page 239, doi:10.3390/E21030239.

[39] J. Miao, C.E. Slone, T.M. Smith, C. Niu, H. Bei, M. Ghazisaeidi, G.M. Pharr, M.J. Mills, The evolution of the deformation substructure in a Ni-Co-Cr equiatomic solid solution alloy, Acta Mater. 132 (2017) 35–48, doi:10.1016/j.actamat.2017.04.033.

[40] J.Q. Zhao, H. Tian, Z. Wang, X.J. Wang, J.W. Qiao, FCC-to-HCP phase transformation in CoCrNix medium-entropy alloys, Acta Metall. Sin. 33 (2020) 1151–1158 (English Letters) 2020 33:8, doi:10.1007/S40195-020-01080-6.

[41] F. Yuan, W. Cheng, S. Zhang, X. Liu, X. Wu, Atomistic simulations of tensile deformation in a CrCoNi medium-entropy alloy with heterogeneous grain structures, Materialia 9 (2020) (Oxf), doi:10.1016/J.MTLA.2019.100565.

[42] C.E. Slone, S. Chakraborty, J. Miao, E.P. George, M.J. Mills, S.R. Niezgoda, Influence of deformation induced nanoscale twinning and FCC-HCP transformation on hardening and texture development in medium-entropy CrCoNi alloy, Acta Mater. 158 (2018) 38–52, doi:10.1016/J.ACTAMAT.2018.07.028.

[43] O. Grässel, L. Krüger, G. Frommeyer, L.W. Meyer, High strength Fe–Mn–(Al, Si) TRIP/TWIP steels development — properties — application, Int. J. Plast. 16 (2000) 1391–1409, doi:10.1016/S0749-6419(00)00015-2.

[44] Y. Chen, D. Chen, X. An, Y. Zhang, Z. Zhou, S. Lu, P. Munroe, S. Zhang, X. Liao, T. Zhu, Z. Xie, Unraveling dual phase transformations in a CrCoNi medium-entropy alloy, Acta Mater. 215 (2021) 117112, doi:10.1016/J.ACTAMAT.2021.117112.

[45] Y. Chen, X. An, Z. Zhou, P. Munroe, S. Zhang, X. Liao, Z. Xie, Size-dependent deformation behavior of dual-phase, nanostructured CrCoNi medium-entropy alloy, Sci. China Mater. 64 (2020) 209–222 2020 64:1, doi:10.1007/S40843-020-1377-2.

[46] L.J. Santodonato, Y. Zhang, M. Feygenson, C.M. Parish, M.C. Gao, R.J.K. Weber, J.C. Neuefeind, Z. Tang, P.K. Liaw, Deviation from high-entropy configurations in the atomic distributions of a multi-principal-element alloy, Nat. Commun. 6 (2015) 1–13 2015 6:1, doi:10.1038/ncomms6964.

[47] Y. Wu, F. Zhang, X. Yuan, H. Huang, X. Wen, Y. Wang, M. Zhang, H. Wu, X. Liu, H. Wang, S. Jiang, Z. Lu, Short-range ordering and its effects on mechanical properties of high-entropy alloys, J. Mater. Sci. Technol. 62 (2021) 214, doi:10.1016/J.JMST.2020.06.018.

[48] L. Zhou, Q. Wang, J. Wang, X. Chen, P. Jiang, H. Zhou, F. Yuan, X. Wu, Z. Cheng, E. Ma, Atomic-scale evidence of chemical short-range order in CrCoNi medium-entropy alloy, Acta Mater. 224 (2022) 117490, doi:10.1016/J.ACTAMAT.2021.117490.

[49] F.X. Zhang, S. Zhao, K. Jin, H. Xue, G. Velisa, H. Bei, R. Huang, J.Y.P. Ko, D.C. Pagan, J.C. Neuefeind, W.J. Weber, Y. Zhang, Local structure and short-range order in a NiCoCr solid solution alloy, Phys. Rev. Lett. 118 (2017) 205501, doi:10.1103/PhysRevLett.118.205501.

[50] R. Zhang, S. Zhao, J. Ding, Y. Chong, T. Jia, C. Ophus, M. Asta, R.O. Ritchie, A.M. Minor, Short-range order and its impact on the CrCoNi medium-entropy alloy, Nature 581 (2020) 283–287, doi:10.1038/s41586-020-2275-z.

[51] A. Tamm, A. Aabloo, M. Klintenberg, M. Stocks, A. Caro, Atomic-scale properties of Ni-based FCC ternary, and quaternary alloys, Acta Mater. 99 (2015) 307–312, doi:10.1016/J.ACTAMAT.2015.08.015.

[52] F. Walsh, M. Asta, R.O. Ritchie, Magnetically driven short-range order can explain anomalous measurements in CrCoNi, Proc. Natl. Acad. Sci. USA 118 (2020), doi:10.1073/pnas.2020540118.

[53] J. Ding, Q. Yu, M. Asta, R.O. Ritchie, Tunable stacking fault energies by tailoring local chemical order in CrCoNi medium-entropy alloys, Proc. Natl. Acad. Sci. USA 115 (2018) 8919–8924, doi:10.1073/pnas.1808660115.

[54] Y. Ikeda, F. Körmann, I. Tanaka, J. Neugebauer, Impact of chemical fluctuations on stacking fault energies of CrCoNi and CrMnFeCoNi high entropy alloys from first principles, Entropy 20 (2018) 655, doi:10.3390/e20090655.

[55] Q.J. Li, H. Sheng, E. Ma, Strengthening in multi-principal element alloys with local-chemical-order roughened dislocation pathways, Nat. Commun. 10 (2019) 1–11 2019 10:1, doi:10.1038/s41467-019-11464-7.

[56] E. Antillon, C. Woodward, S.I. Rao, B. Akdim, T.A. Parthasarathy, Chemical short range order strengthening in a model FCC high entropy alloy, Acta Mater. 190 (2020) 29–42, doi:10.1016/J.ACTAMAT.2020.02.041.

[57] B. Yin, S. Yoshida, N. Tsuji, W.A. Curtin, Yield strength and misfit volumes of NiCoCr and implications for short-range-order, Nat. Commun. 11 (2020) 1–7 2020 11:1, doi:10.1038/s41467-020-16083-1.

[58] Z. Zhang, H. Sheng, Z. Wang, B. Gludovatz, Z. Zhang, E.P. George, Q. Yu, S.X. Mao, R.O. Ritchie, Dislocation mechanisms and 3D twin architectures generate exceptional strength-ductility-toughness combination in CrCoNi medium-entropy alloy, Nat. Commun. 8 (2017) 1–8 2017 8:1, doi:10.1038/ncomms14390.

[59] P. Cao, How does short-range order impact defect kinetics in irradiated multiprincipal element alloys? Acc. Mater. Res. 2 (2021) 71–74, doi:10.1021/ACCOUNTSMR.0C00102.

[60] M. Yang, D. Yan, F. Yuan, P. Jiang, E. Ma, X. Wu, Dynamically reinforced heterogeneous grain structure prolongs ductility in a medium-entropy alloy with gigapascal yield strength, Proc. Natl. Acad. Sci. 115 (2018) 7224–7229, doi:10.1073/PNAS.1807817115.

[61] L. Zhang, X. Du, L. Zhang, W. Li, Y. Liang, J. Yu, N. Zou, G. Wan, Y. Tang, G. Duan, B. Wu, Achieving ultra-high strength in a precipitation-hardened CoCrNi-based medium-entropy alloy with partially recrystallized microstructure and heterogeneous grains, Vacuum 188 (2021) 110169, doi:10.1016/J.VACUUM.2021.110169.

[62] Y. Ma, M. Yang, F. Yuan, X. Wu, Deformation induced hcp nano-lamella and its size effect on the strengthening in a CoCrNi medium-entropy alloy, Jo. Mater. Sci. Technol. 82 (2021) 122–134, doi:10.1016/J.JMST.2020.12.017.

[63] G. Dan Sathiaraj, W. Skrotzki, A. Pukenas, R. Schaarschuch, R. Jose Immanuel, S.K. Panigrahi, J. Arout Chelvane, S.S. Satheesh Kumar, Effect of annealing on

[64] P. Sathiyamoorthi, P. Asghari-Rad, J.W. Bae, H.S. Kim, Fine tuning of tensile properties in CrCoNi medium entropy alloy through cold rolling and annealing, Intermetallics 113 (2019) 106578 (Barking), doi:10.1016/J.INTERMET.2019.106578.

[65] J. Saha, P.P. Bhattacharjee, Influences of thermomechanical processing by severe cold and warm rolling on the microstructure, texture, and mechanical properties of an equiatomic CoCrNi medium-entropy alloy, J. Mater. Eng. Perform. 2021 (2021) 1–16, doi:10.1007/S11665-021-06092-6.

[66] Y. Ma, F. Yuan, M. Yang, P. Jiang, E. Ma, X. Wu, Dynamic shear deformation of a CrCoNi medium-entropy alloy with heterogeneous grain structures, Acta Mater. 148 (2018) 407–418, doi:10.1016/J.ACTAMAT.2018.02.016.

[67] C.E. Slone, J. Miao, E.P. George, M.J. Mills, Achieving ultra-high strength and ductility in equiatomic CrCoNi with partially recrystallized microstructures, Acta Mater. 165 (2019) 496–507, doi:10.1016/J.ACTAMAT.2018.12.015.

[68] X. Zheng, W. Xie, L. Zeng, H. Wei, X. Zhang, H. Wang, Achieving high strength and ductility in a heterogeneous-grain-structured CrCoNi alloy processed by cryorolling and subsequent short-annealing, Mater. Sci. Eng. A 821 (2021) 141610, doi:10.1016/J.MSEA.2021.141610.

[69] Y. Liu, Y. He, S. Cai, Effect of gradient microstructure on the strength and ductility of medium-entropy alloy processed by severe torsion deformation, Mater. Sci. Eng. A 801 (2021) 140429, doi:10.1016/J.MSEA.2020.140429.

[70] S. Praveen, J.W. Bae, P. Asghari-Rad, J.M. Park, H.S. Kim, Annealing-induced hardening in high-pressure torsion processed CoCrNi medium entropy alloy, Mater. Sci. Eng. A 734 (2018) 338–340, doi:10.1016/J.MSEA.2018.07.107.

[71] P. Sathiyamoorthi, J.W. Bae, P. Asghari-Rad, J.M. Park, J.G. Kim, H.S. Kim, Effect of annealing on microstructure and tensile behavior of CoCrNi medium entropy alloy processed by high-pressure torsion, Entropy 20 (2018) 849 2018, Vol. 20, Page 849, doi:10.3390/E20110849.

[72] S. Yoshida, T. Bhattacharjee, Y. Bai, N. Tsuji, Friction stress and Hall-Petch relationship in CoCrNi equi-atomic medium entropy alloy processed by severe plastic deformation and subsequent annealing, Scr. Mater. 134 (2017) 33–36, doi:10.1016/J.SCRIPTAMAT.2017.02.042.

[73] B. Schuh, R. Pippan, A. Hohenwarter, Tailoring bimodal grain size structures in nanocrystalline compositionally complex alloys to improve ductility, Mater. Sci. Eng. A 748 (2019) 379–385, doi:10.1016/J.MSEA.2019.01.073.

[74] Y. Liu, G. He, Y. Yang, K. Li, H. Gong, B. Gan, C. Huang, Revealing the microstructural evolution and mechanism during the thermomechanical treatment of polycrystalline CrCoNi medium-entropy alloy, J. Alloy. Compd. 870 (2021) 159518, doi:10.1016/J.JALLCOM.2021.159518.

[75] B. Gan, J.M. Wheeler, Z. Bi, L. Liu, J. Zhang, H. Fu, Superb cryogenic strength of equiatomic CrCoNi derived from gradient hierarchical microstructure, J. Mater. Sci. Technol. 35 (2019) 957–961, doi:10.1016/J.JMST.2018.12.002.

[76] A. Kishore, M. John, A.M. Ralls, S.A. Jose, U.B. Kuruveri, P.L. Menezes, Ultrasonic nanocrystal surface modification: processes, characterization, properties, and applications, Nanomaterials 12 (2022) 1415 2022, Vol. 12, Page 1415, doi:10.3390/NANO12091415.

[77] J.G. Kim, J.H. Moon, A. Amanov, H.S. Kim, Strength and ductility enhancement in the gradient structured twinning-induced plasticity steel by ultrasonic nanocrystalline surface modification, Mater. Sci. Eng. A 739 (2019) 105–108, doi:10.1016/J.MSEA.2018.10.045.

[78] C. Ye, A. Telang, A.S. Gill, S. Suslov, Y. Idell, K. Zweiacker, J.M.K. Wiezorek, Z. Zhou, D. Qian, S.R. Mannava, V.K. Vasudevan, Gradient nanostructure and residual stresses induced by ultrasonic nano-crystal surface modification in 304 austenitic stainless steel for high strength and high ductility, Mater. Sci. Eng. A 613 (2014) 274–288, doi:10.1016/J.MSEA.2014.06.114.

[79] T.A. Listyawan, H. Lee, N. Park, U. Lee, Microstructure and mechanical properties of CoCrFeMnNi high entropy alloy with ultrasonic nanocrystal surface modification process, J. Mater. Sci. Technol. 57 (2020) 123–130, doi:10.1016/J.JMST.2020.02.083.

[80] H.H. Lee, H.K. Park, J. Jung, A. Amanov, H.S. Kim, Multi-layered gradient structure manufactured by single-roll angular-rolling and ultrasonic nanocrystalline surface modification, Scr. Mater. 186 (2020) 52–56, doi:10.1016/J.SCRIPTAMAT.2020.03.051.

[81] J.W. Bae, P. Asghari-Rad, A. Amanov, H.S. Kim, Gradient-structured ferrous medium-entropy alloys with enhanced strength-ductility synergy by ultrasonic nanocrystalline surface modification, Mater. Sci. Eng. A 826 (2021) 141966, doi:10.1016/J.MSEA.2021.141966.

[82] K.M. Rahman, V.A. Vorontsov, D. Dye, The effect of grain size on the twin initiation stress in a TWIP steel, Acta Mater. 89 (2015) 247–257, doi:10.1016/J.ACTAMAT.2015.02.008.

[83] W.Z. Han, Z.F. Zhang, S.D. Wu & S.X. Li, Combined effects of crystallographic orientation, stacking fault energy and grain size on deformation twinning in fcc crystals, Philosophical Magazine. 88:24 (2008) 3011-3029, doi: 10.1080/14786430802438168

[84] G.W. Hu, L.C. Zeng, H. Du, X.W. Liu, Y. Wu, P. Gong, Z.T. Fan, Q. Hu, E.P. George, Tailoring grain growth and solid solution strengthening of single-phase CrCoNi medium-entropy alloys by solute selection, J. Mater. Sci. Technol. 54 (2020) 196–205, doi:10.1016/J.JMST.2020.02.073.

[85] O.N. Senkov, D.B. Miracle, Effect of the atomic size distribution on glass forming ability of amorphous metallic alloys, Mater. Res. Bull. 36 (2001) 2183–2198, doi:10.1016/S0025-5408(01)00715-2.

[86] M.P. Agustianingrum, S. Yoshida, N. Tsuji, N. Park, Effect of aluminum addition on solid solution strengthening in CoCrNi medium-entropy alloy, J. Alloy. Compd. 781 (2019) 866–872, doi:10.1016/J.JALLCOM.2018.12.065.

[87] D. Lee, M.P. Agustianingrum, N. Park, N. Tsuji, Synergistic effect by Al addition in improving mechanical performance of CoCrNi medium-entropy alloy, J. Alloy. Compd. 800 (2019) 372–378, doi:10.1016/J.JALLCOM.2019.06.005.

[88] W. Lu, X. Luo, Y. Yang, J. Zhang, B. Huang, Effects of Al addition on structural evolution and mechanical properties of the CrCoNi medium-entropy alloy, Mater. Chem. Phys. 238 (2019) 121841, doi:10.1016/J.MATCHEMPHYS.2019.121841.

[89] P. Sathiyamoorthi, J.M. Park, J. Moon, J.W. Bae, P. Asghari-Rad, A. Zargaran, H. Seop Kim, Achieving high strength and high ductility in Al$_{0.3}$CoCrNi medium-entropy alloy through multi-phase hierarchical microstructure, Materialia 8 (2019) 100442 (Oxf), doi:10.1016/J.MTLA.2019.100442.

[90] Superalloys: a primer and history, (n.d.). https://www.tms.org/meetings/specialty/superalloys2000/superalloyshistory.html (accessed October 4, 2021).

[91] Y.L. Zhao, T. Yang, Y. Tong, J. Wang, J.H. Luan, Z.B. Jiao, D. Chen, Y. Yang, A. Hu, C.T. Liu, J.J. Kai, Heterogeneous precipitation behavior and stacking-fault-mediated deformation in a CoCrNi-based medium-entropy alloy, Acta Mater. 138 (2017) 72–82, doi:10.1016/J.ACTAMAT.2017.07.029.

[92] Y. Zhao, T. Yang, B. Han, J. Luan, D. Chen, W. Kai, C.T. Liu, J. Kai, Exceptional nanostructure stability and its origins in the CoCrNi-based precipitation-strengthened medium-entropy alloy, Materials Research Letters. 7:4 (2019) 152-158, doi:10.1080/21663831.2019.1568315.

[93] N. Guo, Y. Zhao, S. Long, B. Song, J. Hu, B. Gan, L. Chai, S. Guo, Microstructure and mechanical properties of (CrCoNi)$_{97}$Al$_{1.5}$Ti$_{1.5}$ medium entropy alloy twisted by free-end-torsion at room and cryogenic temperatures, Mater. Sci. Eng. A 797 (2020) 140101, doi:10.1016/J.MSEA.2020.140101.

[94] C.E. Slone, C.R. LaRosa, C.H. Zenk, E.P. George, M. Ghazisaeidi, M.J. Mills, Deactivating deformation twinning in medium-entropy CrCoNi with small additions of aluminum and titanium, Scr. Mater. 178 (2020) 295–300, doi:10.1016/J.SCRIPTAMAT.2019.11.053.

[95] X.W. Liu, G. Laplanche, A. Kostka, S.G. Fries, J. Pfetzing-Micklich, G. Liu, E.P. George, Columnar to equiaxed transition and grain refinement of cast CrCoNi medium-entropy alloy by microalloying with titanium and carbon, J. Alloy. Compd. 775 (2019) 1068–1076, doi:10.1016/j.jallcom.2018.10.187.

[96] R. Chang, W. Fang, J. Yan, H. Yu, X. Bai, J. Li, S. Wang, S. Zheng, F. Yin, Microstructure and mechanical properties of CoCrNi-Mo medium entropy alloys: experiments and first-principle calculations, J. Mater. Sci. Technol. 62 (2021) 25–33, doi:10.1016/j.jmst.2020.04.062.

[97] R. Chang, W. Fang, H. Yu, X. Bai, X. Zhang, B. Liu, F. Yin, Heterogeneous banded precipitation of (CoCrNi)$_{93}$Mo$_7$ medium entropy alloys towards strength–ductility synergy utilizing compositional inhomogeneity, Scr. Mater. 172 (2019) 144–148, doi:10.1016/J.SCRIPTAMAT.2019.07.026.

[98] N. Li, J. Gu, B. Gan, Q. Qiao, S. Ni, M. Song, Effects of Mo-doping on the microstructure and mechanical properties of CoCrNi medium entropy alloy, J. Mater. Res. 35 (2020) 2726–2736 2020 35:20, doi:10.1557/JMR.2020.256.

[99] J. Miao, T. Guo, J. Ren, A. Zhang, B. Su, J. Meng, Optimization of mechanical and tribological properties of FCC CrCoNi multi-principal element alloy with Mo addition, Vacuum 149 (2018) 324–330, doi:10.1016/J.VACUUM.2018.01.012.

[100] X. Liu, M. Zhang, Y. Ma, W. Dong, R. Li, Y. Lu, Y. Zhang, P. Yu, Y. Gao, G. Li, Achieving ultrahigh strength in CoCrNi-based medium-entropy alloys with synergistic strengthening effect, Mater. Sci. Eng. A 776 (2020) 139028, doi:10.1016/J.MSEA.2020.139028.

[101] Z. Wu, W. Guo, K. Jin, J.D. Poplawsky, Y. Gao, H. Bei, Enhanced strength and ductility of a tungsten-doped CoCrNi medium-entropy alloy, J. Mater. Res. 33 (2018) 3301–3309 2018 33:19, doi:10.1557/JMR.2018.247.

[102] R. Chang, W. Fang, X. Bai, C. Xia, X. Zhang, H. Yu, B. Liu, F. Yin, Effects of tungsten additions on the microstructure and mechanical properties of CoCrNi medium entropy alloys, J. Alloy. Compd. 790 (2019) 732–743, doi:10.1016/J.JALLCOM.2019.03.235.

[103] S.M. Lee, S.J. Lee, S. Lee, J.H. Nam, Y.K. Lee, Tensile properties and deformation mode of Si-added Fe-18Mn-0.6C steels, Acta Mater. 144 (2018) 738–747, doi:10.1016/J.ACTAMAT.2017.11.023.

[104] H. Chang, T.W. Zhang, S.G. Ma, D. Zhao, R.L. Xiong, T. Wang, Z.Q. Li, Z.H. Wang, Novel Si-added CrCoNi medium entropy alloys achieving the breakthrough of strength-ductility trade-off, Mater. Des. 197 (2021) 109202, doi:10.1016/J.MATDES.2020.109202.

[105] S. Liu, W. Lin, Y. Zhao, D. Chen, G. Yeli, F. He, S. Zhao, J. Jung Kai, Effect of silicon addition on the microstructures, mechanical properties and helium irradiation resistance of NiCoCr-based medium-entropy alloys, J. Alloy. Compd. 844 (2020) 156162, doi:10.1016/J.JALLCOM.2020.156162.

[106] H. Yi, M. Bi, K. Yang, B. Zhang, Significant Improvement the mechanical properties of CoCrNi alloy by tailoring a dual FCC-phase structure, Materials 13 (2020) 4909 2020, Vol. 13, Page 4909, doi:10.3390/MA13214909.

[107] S. Asgari, Age-hardening behavior and phase identification in solution-treated AEREX 350 superalloy, Metall. Mater. Trans. A 37 (2006) 2051–2057 2006 37:7, doi:10.1007/BF02586125.

[108] M. Kermajani, Influence of double aging on microstructure and yield strength of AEREX^{TM} 350, Mater. Sci. Eng. A 534 (2012) 547–551, doi:10.1016/J.MSEA.2011.12.006.

[109] R. Cosimati, D. Mari, Secondary hardening in Co-Ni-Cr super-alloy investigated by mechanical spectroscopy, Mater. Sci. Eng. A 662 (2016) 426–431, doi:10.1016/J.MSEA.2016.03.091.

[110] L.U. Shioiang, B. Shang, Z. Luo, R. Wang, F. Zeng, Investigation on the cold deformation strengthening mechanism in MP159 alloy, Metall. Mater. Trans. A 31 (2000) 5–13 2000 31:1, doi:10.1007/S11661-000-0046-X.

[111] J. Gu, B. Gan, Z. Bi, M. Song, Microstructure and mechanical properties of a MP159 superalloy after pre-tensile deformation and subsequent annealing, Adv. Eng. Mater. (2021) 2100920, doi:10.1002/ADEM.202100920.

[112] I.S. Demchuk, V.I. Krakhmalev, D.V. Lebedev, Creep of cryogenic steels and alloys, Met. Sci. Heat Treat. 21 (1979) 547–553 1980 21:7, doi:10.1007/BF00703668.

[113] B. Fultz, A. DuBois, H.J. Kim, J.W. Morris, Cryogenic mechanical properties of superalloy MP35N, Cryogenics 24 (1984) 687–690 (Guildf), doi:10.1016/0011-2275(84)90040-7.

[114] M. Farvizi, S. Asgari, Effects of cold work prior to aging on microstructure of AEREX^{TM}350 superalloy, Mater. Sci. Eng. A 480 (2008) 434–438, doi:10.1016/J.MSEA.2007.07.052.

[115] Y. Koizumi, S. Suzuki, K. Yamanaka, B.S. Lee, K. Sato, Y. Li, S. Kurosu, H. Matsumoto, A. Chiba, Strain-induced martensitic transformation near twin boundaries in a biomedical Co–Cr–Mo alloy with negative stacking fault energy, Acta Mater. 61 (2013) 1648–1661, doi:10.1016/J.ACTAMAT.2012.11.041.

[116] E.M. Shaji, S.R. Kalidindi, R.D. Doherty, Influence of cold-work and aging heat treatment on strength and ductility of MP35N, Mater. Sci. Eng. A 272 (1999) 371–379, doi:10.1016/S0921-5093(99)00502-X.

[117] D. Sorensen, B.Q. Li, W.W. Gerberich, K.A. Mkhoyan, Investigation of secondary hardening in Co–35Ni–20Cr–10Mo alloy using analytical scanning transmission electron microscopy, Acta Mater. 63 (2014) 63–72, doi:10.1016/J.ACTAMAT.2013.10.005.

[118] V.J. Toplosky, K. Han, Mechanical properties of cold-rolled and aged MP35N alloys for cryogenic magnet applications, AIP Conf. Proc. 1435 (2012) 125, doi:10.1063/1.4712088.

[119] A. Ishmaku, Ke. Han, Deformation induced Nanostructure and texture in MP35N alloys, Journal of Materials Science 39 (2004) 5417–5420, doi:10.1023/B:JMSC.0000039257.96990.c6.

[120] E.M. Shaji, S.R. Kalidindi, R.D. Doherty, A.S. Sedmak, Fracture properties of multiphase alloy MP35N, Mater. Sci. Eng. A 349 (2003) 313–317, doi:10.1016/S0921-5093(02)00809-2.

[121] Q. Luo, H.H. Wang, G.Q. Li, C. Sun, D.H. Li, X.L. Wan, On mechanical properties of novel high-Mn cryogenic steel in terms of SFE and microstructural evolution, Mater. Sci. Eng. A 753 (2019) 91–98, doi:10.1016/J.MSEA.2019.02.093.

[122] M.J.N.V. Prasad, M.W. Reiterer, K.S. Kumar, Microstructure and mechanical behavior of annealed MP35N alloy wire, Mater. Sci. Eng. A 636 (2015) 340–351, doi:10.1016/J.MSEA.2015.03.103.

[123] G.W. Han, I.P. Jones, R.E. Smallman, Direct evidence for Suzuki segregation and Cottrell pinning in MP159 superalloy obtained by FEG(S)TEM/EDX, Acta Mater. 51 (2003) 2731–2742, doi:10.1016/S1359-6454(02)00359-2.

[124] Samiee, Mojtaba & Asgari, Sirous. (2008). A TEM investigation on precipitation behavior of AEREX350 superalloy. Proceedings of the International Symposium on Superalloys. 549-552. doi:10.7449/2008/Superalloys_2008_549_552.

[125] M. Kermajani, Influence of double aging on microstructure and yield strength of AEREX^{TM} 350, Mater. Sci. Eng. A 534 (2012) 547–551, doi:10.1016/J.MSEA.2011.12.006.

[126] T.M. Smith, M.S. Hooshmand, B.D. Esser, F. Otto, D.W. Mccomb, E.P. George, M. Ghazisaeidi, M.J. Mills, Atomic-scale characterization and modeling of 60° dislocations in a high-entropy alloy, Acta Mater. 110 (2016) 352–363, doi:10.1016/J.ACTAMAT.2016.03.045.

[127] M. Shih, J. Miao, M. Mills, M. Ghazisaeidi, Stacking fault energy in concentrated alloys, Nat. Commun. 12 (2021) 1–10 2021 12:1, doi:10.1038/s41467-021-23860-z.

[128] Elgiloy alloy - strip division | elgiloy specialty metals, (n.d.). https://www.elgiloy.com/strip-elgiloy-alloy/(accessed March 27, 2022).

[129] Haynes alloy 188, (n.d.). https://www.americanspecialmetals.com/Haynes188Alloy.html (accessed March 27, 2022).

[130] AISI HS31-X40-X45 cobalt alloys: chemical composition & other alloy properties, (n.d.). https://alloytester.com/alloyapp/family/grade/product/249-aisi (accessed March 27, 2022).

[131] Haynes International- Principal Features, (n.d.). https://www.haynesintl.com/alloys/alloy-portfolio_/High-temperature-Alloys/HAYNES263alloyportfolio/principal-features.aspx (accessed June 21, 2022).

[132] MAR-M 432 Valve,MAR-M 432 flanges,MAR-M 432 Pipe Fitting,MAR-M 432 Reducer,MAR-M 432 Angle Bar,MAR-M 432 Pipe,Pipe Tee, (n.d.). https://www.yaang.com/data-center/High-alloy/mar-m-432.html (accessed March 27, 2022).

[133] NIMONIC® alloy 105, (n.d.). https://www.specialmetals.com/documents/technical-bulletins/nimonic-alloy-105.pdf (accessed March 27, 2022).

[134] Super alloy Udimet 500TM (UNS N07500), (n.d.). https://www.azom.com/article.aspx?ArticleID=7738 (accessed March 27, 2022).

[135] Special metals Udimet® 700 nickel alloy, (n.d.). https://www.matweb.com/search/datasheet.aspx?matguid=42b0db30b54e4e46aed918c32cab0b26&ckck=1 (accessed March 27, 2022).

[136] Nickel-based IN939 alloy, (n.d.). https://www.slm-solutions.com/fileadmin/Content/Powder/MDS/MDS_Ni-Alloy_IN939_0219_EN.pdf

[137] Nimonic 90 data sheet, (n.d.). https://www.quest4alloys.com/product-range/nickel-alloys/2-content/163-nimonic-90-data-sheet (accessed March 27, 2022).

[138] Super alloy Nimonic 115TM, (n.d.). https://www.azom.com/article.aspx?ArticleID=7841 (accessed March 27, 2022).

[139] Super alloy Nimonic PK33TM, (n.d.). https://www.azom.com/article.aspx?ArticleID=7706 (accessed March 27, 2022).

[140] INCONEL ® alloy 617, (n.d.). https://www.specialmetals.com/documents/technical-bulletins/inconel/inconel-alloy-617.pdf.

[141] Rene 41 - Premium Cobalt Alloys from NeoNickel, (n.d.). https://www.neonickel.com/alloys/nickel-alloys/rene-41/ (accessed June 21, 2022).